

**INSTITUTO POLITÉCNICO NACIONAL**  
**Centro de Investigación en Ciencia Aplicada**  
**y Tecnología Avanzada Unidad Legaria**



Studies of the active sites in copper exchanged mordenite with  
applications in Methane to Methanol conversion

TESIS

TESIS QUE PARA OBTENER EL GRADO DE  
**MAESTRO EN TECNOLOGÍA AVANZADA**

PRESENTA

**HEBERT RODRIGO MOJICA MOLINA**

CIUDAD DE MÉXICO

JULIO 2019



**INSTITUTO POLITÉCNICO NACIONAL**  
**SECRETARIA DE INVESTIGACIÓN Y POSGRADO**

SIP-13  
REP 2017

*ACTA DE REGISTRO DE TEMA DE TESIS  
Y DESIGNACIÓN DE DIRECTOR DE TESIS*

Ciudad de México,  de  del

El Colegio de Profesores de Posgrado de  en su Sesión  
(Unidad Académica)

No.  celebrada el día  del mes  de  conoció la solicitud presentada por el (la) alumno (a):

Apellido Paterno:	<b>Mojica</b>	Apellido Materno:	<b>Molina</b>	Nombre (s):	<b>Hebert Rodrigo</b>
-------------------	---------------	-------------------	---------------	-------------	-----------------------

Número de registro:

del Programa Académico de Posgrado:

Referente al registro de su tema de tesis; acordando lo siguiente:

1.- Se designa al aspirante el tema de tesis titulado:

Objetivo general del trabajo de tesis:

2.- Se designa como Directores de Tesis a los profesores:

Director:  2° Director:   
No aplica:

3.- El Trabajo de investigación base para el desarrollo de la tesis será elaborado por el alumno en:

que cuenta con los recursos e infraestructura necesarios.

4.- El interesado deberá asistir a los seminarios desarrollados en el área de adscripción del trabajo desde la fecha en que se suscribe la presente, hasta la aprobación de la versión completa de la tesis por parte de la Comisión Revisora correspondiente.

Director(a) de Tesis  
  
Dr. Edilso Francisco Reguera Ruíz  
Aspirante  
  
Lic. Hebert Rodrigo Mojica Molina

2° Director de Tesis (en su caso)  
  
Dra. Marlene González Montiel  
Presidente del Colegio  
  
Dra. Mónica Rosalía Jaime Fonseca  
  
CENTRO DE INVESTIGACIÓN EN CIENCIA  
APLICADA Y TECNOLOGÍA AVANZADA  
CICATA - LEGARIA  
Página 1 de 1



# INSTITUTO POLITÉCNICO NACIONAL

## SECRETARÍA DE INVESTIGACIÓN Y POSGRADO

### ACTA DE REVISIÓN DE TESIS

En la Ciudad de  siendo las  horas del día  del mes de  del  se reunieron los miembros de la Comisión Revisora de la Tesis, designada por el Colegio de Profesores de Posgrado de:  para examinar la tesis titulada:  por el (la) alumno (a):

Apellido Paterno:	<b>Mojica</b>	Apellido Materno:	<b>Molina</b>	Nombre (s):	<b>Hebert Rodrigo</b>
-------------------	---------------	-------------------	---------------	-------------	-----------------------

Número de registro:

Aspirante del Programa Académico de Posgrado:

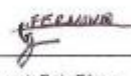
Después de la lectura y revisión individual, así como el análisis e intercambio de opiniones, los miembros de la Comisión manifestaron **APROBAR**  **NO APROBAR**  la tesis, en virtud de los motivos siguientes:

Los objetivos propuestos fueron bien planteados y alcanzados, las técnicas de caracterización utilizadas son adecuadas para explicar, a través de una redacción clara, los fenómenos que la tesis propone estudiar.

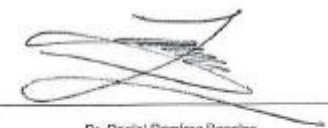
#### Comisión Revisora de Tesis

  
 Dr. Ediso Francisco Reguera Ruiz  
 Director de Tesis  
 12103-EE-16 Profesor Colegiado

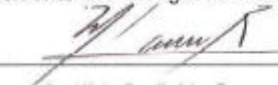
  
 Dra. Zeneida Carolina Leyva Ivanza  
 13098-EB-18 Profesor Colegiado

  
 Dr. Fernando Trépo Zárraga  
 12895-ED-17 Profesor Colegiado

  
 Dra. Mariene González Montiel  
 2º Director de Tesis  
 14296-EB-19 Profesor Visitante

  
 Dr. Daniel Ramírez Rosales  
 11719-EE-16 Profesor Visitante

#### Presidente del Colegio de Profesores

  
 Dra. Mónica Rosalva Jaime Fonseca



SEP  
CENTRO DE INVESTIGACIÓN EN CIENCIA  
APLICADA Y TECNOLOGÍA AVANZADA  
CICATA - LEGARIA



**INSTITUTO POLITÉCNICO NACIONAL**  
**SECRETARÍA DE INVESTIGACIÓN Y POSGRADO**

**CARTA CESIÓN DE DERECHOS**

En la Ciudad de México el día 12 del mes Junio del año 2019, el que suscribe Hebert Rodrigo Mojica Molina alumno del Programa de Maestría en Tecnología Avanzada con número de registro B170517, adscrito al Centro de Investigación en Ciencia Aplicada y Tecnología Avanzada Unidad Legaria CICATA-Legaria, manifiesta que es autor intelectual del presente trabajo de Tesis bajo la dirección de Dr. Edilso Francisco Reguera Ruiz y Dra. Marlene González Montiel y cede los derechos del trabajo intitulado Studies of the active sites in copper exchanged mordenite with applications in methane to methanol conversion, al Instituto Politécnico Nacional para su difusión, con fines académicos y de investigación.

Los usuarios de la información no deben reproducir el contenido textual, gráficas o datos del trabajo sin el permiso expreso del autor y/o director del trabajo. Este puede ser obtenido escribiendo a la siguiente dirección rodrigo1993mx@gmail.com. Si el permiso se otorga, el usuario deberá dar el agradecimiento correspondiente y citar la fuente del mismo.

Hebert Rodrigo Mojica Molina.

## CONTENT

<b>ACKNOWLEDGMENT.</b> .....	8
<b>RESUMEN.</b> .....	9
<b>ABSTRACT</b> .....	11
<b>INTRODUCTION</b> .....	12
<b>HYPOTHESIS</b> .....	13
<b>OBJECTIVES</b> .....	13
<b>1. THEORETICAL FRAMEWORK.</b> .....	14
<b>1.1 The Context and Physical-Chemical Features of Methane.</b> .....	14
<b>1.2 Valorization of Methane.</b> .....	15
<b>1.3 Methanol from Methane, a Fundamental Issue.</b> .....	16
<b>1.4 Methane Monooxygenase.</b> .....	17
<b>1.5 Current Technologies to Obtain Methanol from Methane.</b> .....	18
<i>1.5.1 Direct conversion of methane to methanol via conventional catalytic processes.</i> .....	19
<i>1.5.2 Homogeneous Radical Gas-Phase Reactions.</i> .....	19
<i>1.5.3 Heterogeneous Catalysis at Mild Conditions.</i> .....	19
<i>1.5.4 Homogeneous Catalysis in Solution.</i> .....	20
<i>1.5.5 Bio-Catalysis Based on Enzymes.</i> .....	21
<i>1.5.6 Plasma Technologies.</i> .....	21
<i>1.5.7 Photo-Catalysis Technologies.</i> .....	21
<i>1.5.8 Supercritical Water Technologies.</i> .....	22
<i>1.5.9 Biological Technology (Membranes).</i> .....	22
<i>1.5.10 Other Technologies for Methane to Methanol Conversion.</i> .....	22
<b>1.6 Copper-Mordenite Based Technologies.</b> .....	23
<b>1.6.1 Zeolite Framework: Mordenite.</b> .....	23
<b>1.6.2 Reported Synthesis of Copper Exchanged Mordenites.</b> .....	25
<b>1.6.4 Methane to Methanol Conversion Process.</b> .....	29
<b>1.6.5 Methanol Desorption Process and Regeneration of Activated Material.</b> .....	29
<b>1.7 Analytical Techniques Employed to study the Methane to Methanol Conversion by Copper (II) Exchanged Mordenites.</b> .....	30
<i>1.7.1 Ultraviolet-Visible Spectroscopy.</i> .....	30

1.7.2 Infrared Spectroscopy. ....	31
1.7.3 Electron Paramagnetic Resonance. ....	31
1.7.4 X-Ray Diffraction. ....	33
1.7.5 Gas Chromatography-Mass Spectrometry. ....	33
1.7.6 Adsorption Analysis. ....	34
1.7.7 Thermogravimetric Analysis. ....	35
1.7.8 Scanning Electron Microscopy (SEM)-Electron Dispersive X-Ray Spectroscopy (EDS). ....	35
<b>2. EXPERIMENTAL SECTION. ....</b>	<b>36</b>
<b>2.1. Experimental Design. ....</b>	<b>36</b>
<b>2.2. Synthesis of Materials. ....</b>	<b>37</b>
<b>2.3. Conversion process. ....</b>	<b>38</b>
2.3.1.a) Ionic Copper Exchange. ....	38
2.3.1.b) Calcination Treatment (Activated Materials). ....	39
<b>2.3.2. Reaction with methane. ....</b>	<b>39</b>
<b>2.3.3. Sample Analysis (washing with liquid water). ....</b>	<b>41</b>
<b>2.4 First observations derived from the synthesis pathway. ....</b>	<b>41</b>
<b>3. RESULTS AND DISCUSSION. ....</b>	<b>43</b>
<b>3.1 Catalyst Characterization. ....</b>	<b>43</b>
<b>3.2 X-Ray Diffraction Analysis. ....</b>	<b>46</b>
<b>3.3 Scanning Electron Microscopy-Energy Dispersive X-Ray Spectroscopy. ....</b>	<b>48</b>
<b>3.4. Gas Chromatography-Mass Spectrometry Analysis. ....</b>	<b>50</b>
<b>3.5 Induced Coupled Plasma-Optical Emission Spectroscopy Analysis. ....</b>	<b>56</b>
<b>3.6 Thermogravimetric Analysis. ....</b>	<b>57</b>
<b>3.7 Adsorption Isotherms (BET Method). ....</b>	<b>59</b>
<b>3.8 Fourier Transform Infrared Spectroscopy Analysis. ....</b>	<b>63</b>
<b>3.9 Electron Spectroscopy Analysis. ....</b>	<b>66</b>
<b>4. CONCLUSIONS. ....</b>	<b>71</b>
<b>5. REFERENCES. ....</b>	<b>73</b>
<b>6. APPENDIX. ....</b>	<b>82</b>
Appendix 1. ....	82
Appendix 2. ....	83
Appendix 3. ....	83

Appendix 4.....	84
Appendix 5.....	85
Appendix 6.....	89
Appendix 7.....	90
Appendix 8.....	90
Appendix 9.....	91

## **ACKNOWLEDGMENT.**

The major of thanks to México and its people, without them this work cannot be possible.

To my parents, they know why.

Thanks to Paula, for your words of encouragement and patience at all times.

Special thanks to Dr. Edilso Reguera Ruíz and Dr. Marlene González Montiel for the given support.

To LNCAE for the infrastructure provided to carry out the experiments and analysis.

## RESUMEN.

La conversión de metano a metanol bajo condiciones suaves de reacción ha sido un reto de mucho tiempo para el campo de la catálisis, incluso es considerada uno de los problemas fundamentales en la ingeniería química. Numerosos materiales basados en intercambios iónicos con diferentes metales de transición (particularmente el cobre), los cuales son capaces de estabilizar sitios metálicos activos a la oxidación del metano con selectividad al metanol, se han investigado y estudiado en un intento por emular la actividad catalítica de la metaloenzima monooxigenasa de metano. Las zeolitas proveen un excelente ambiente estructural para la estabilización de sitios activos de cobre para llevar a cabo la reacción de metano a metanol bajo condiciones suaves estáticas y dinámicas. Particularmente la mordenita intercambiada con cobre ha demostrado poseer un excelente ambiente para la formación de sitios activos de cobre estables y una estructura que favorece el tránsito de especies, lo que favorece la dinámica de la reacción de conversión. El principal objetivo de este trabajo es obtener información sobre los sitios activos formados en la mordenita intercambiada con cobre obtenida a través de una síntesis mecano química, y probar estos materiales en la reacción de metano a metanol bajo condiciones suaves y estáticas. Se busca que estos materiales presenten selectividad hacia el metanol, evitando la sobreoxidación hacia óxidos de carbono y agua. Para el estudio del proceso de conversión se emplea un diseño factorial de tres variables (por ciento en peso de cobre, temperatura de activación y presión de metano) en condiciones estáticas. Se encontró que las muestras de 3% en peso de cobre presentan la mayor producción de metanol en comparación con las muestras de 5% y 1% en peso de cobre, en concordancia con el análisis estequiométrico presentado. Por otro lado, temperaturas más altas de activación reflejan una mejora en la formación y reactividad de los sitios activos y una eliminación completa de los residuos asociados a los precursores de cobre. Varios análisis espectroscópicos (UV-Vis, EPR e IR) y por cromatografía de gases acoplada a espectrometría de masas muestran la funcionalidad de la ruta de síntesis y de las condiciones del proceso de conversión empleado a través de la cuantificación del metanol obtenido, la inexistencia del sitio mono-( $\mu$ -oxo) dicobre en las mordenitas intercambiadas y la identificación de un sitio activo probable, no reportado aún. Se identificó el sitio trimer  $[\text{Cu}_3(\mu\text{-O})_3]^{2+}$  en vez del sitio  $[\text{Cu}_2(\mu\text{-O})]^{2+}$ , el cual se propone

como responsable del proceso de conversión de metano a metanol en los materiales sintetizados. El ambiente de coordinación de las especies de cobre y el comportamiento de los iones de cobre a través de el ciclo experimental es discutido mediante la información proporcionada por las técnicas espectroscópicas EPR y UV-Vis. Información adicional proporcionada por más técnicas espectroscópicas y complementarias es discutida también.

## ABSTRACT

The direct conversion of methane to methanol under mild conditions has been a long-standing challenge for the catalysis field. In an attempt to emulate the methane monooxygenase metalloenzyme activity, different copper-based materials have been tested to understand their active methane to methanol conversion sites. Zeolites provide an excellent framework structure to stabilize active copper sites and to carry out the reaction under static or dynamic conditions; particularly copper exchanged Mordenite has demonstrated to provide a good environment for the formation of copper active sites and adequate framework to carry out the methane to methanol conversion. The main aim of this work is to obtain information on the reactive methane sites in copper Mordenite by using a mechano-synthesis pathway and test this material in the methane to methanol conversion under mild and static conditions, trying to reach selectivity towards methanol, avoiding overoxidation. For the study of the conversion process, it is employed a factorial experimental design with three variables (weight percent copper loaded, activation temperature, and pressure of methane) in static conditions. It was found that 3% wt copper loaded mordenite provide higher yields than 5% wt and 1% wt copper, in accordance with stoichiometric calculations. On the other hand, higher calcination temperatures provide better active sites formation/reactivity and a complete residues elimination. Spectroscopic analysis (UV-Vis, EPR and IR) and GC-MS techniques show the functionality of the synthesis method and conversion process employed, by quantifying the obtained methanol, the apparent nonexistence of mono- $\mu$ -oxo dicopper core in mordenite, and the formation of a probable non reported reactive species according to the changes in the studied variables throughout the whole conversion process steps. It is observed trimer  $[\text{Cu}_3(\mu\text{-O})_3]^{2+}$  copper species instead of  $[\text{Cu}_2(\mu\text{-O})]^{2+}$ , which is assumed to be responsible for the conversion process behavior during the methane reaction step under study. The coordination environment of copper species and the behavior of copper ions throughout the experimental cycle is discussed with EPR and UV-Vis Spectroscopies data. Additional spectroscopic and analytical complementary results are also discussed.

## **INTRODUCTION**

The methane to methanol conversion under mild conditions is a significant problem to be solved in the following years, not only for the current environmental global situation (one of the biggest problems that we, as humanity, have to solve in the short term), but also, for the growing need of energy suppliers seeking to satisfy the population demand their basic needs and life quality improvement. The current reserves of natural gas, whose main component is methane, overcome several times the probed oil reserves for the next fifty years; this fact makes unpostponable the development of new technologies that allow the use of methane as a chemical feedstock, for production of added value products without a high energetic and environmental cost. Many efforts have been applied to develop materials that work as a catalyst for the methane oxidation reaction; between them, zeolites exchanged with transition metals (e.g., Copper, Iron, Cobalt, etc.), particularly, the copper exchanged mordenite has demonstrated a good performance in methane to methanol conversion in continuous flow reactors systems; that is why this material will be studied in the present work. Also, the procedure of activation (by calcination) and synthesis pathway (solid-state ion exchange) used herein, showed important changes in the methane yields. Among the current low-cost conversion technologies for obtaining methanol from methane, copper (II) exchanged mordenites presents one of the higher methanol yields, so, important efforts must be applied to enhance it, with prospects for industrial scale. For this purpose, the functioning of the materials must be understood in its entirety by basic and experimental research. In that way, two spectroscopies have been broadly used to study this kind of materials: UV-Vis and EPR spectroscopies, with the purpose to identify the active sites responsible for methane conversion and analyze their behavior in the reaction cycle. Other analytical techniques are employed to shed light about the physical-chemical properties of the materials, which actually are very important for the reaction conditions and for the methanol production results. Copper exchanged mordenites, employed for methane to methanol conversion, provides an opportunity to understand the mechanism that could allow us to develop new materials that produce greater methanol conversion per unit mass.

## **HYPOTHESIS**

Following a mechanochemical synthesis pathway, where the starting materials are ammonium mordenite and copper acetylacetonate, the insertion of copper ions in the structure of the mordenite will be effective; with the consequent formation of stable copper active sites in ambient conditions, for the oxidation of methane to methanol under mild and static reaction conditions.

## **OBJECTIVES**

- **General.**

1. To search for functional materials that can carry out, under mild and static conditions, the methane oxidation towards methanol; based in copper exchanged mordenite procedure.

- **Particular.**

1. To characterize and study these materials with spectroscopical and complementary techniques, in order to determine the nature of the active sites which are responsible for the methane to methanol conversion.
2. To analyze the functionality of the material when reacts with methane by studying the amounts of produced methanol in a designed experiment.

## 1. THEORETICAL FRAMEWORK.

### 1.1 The Context and Physical-Chemical Features of Methane.

For many years the common human activities have required considerable and increasing amounts of energy. At present, energy is mainly acquired from burning fossil fuels. This activity produces contaminant emissions of carbon dioxide, nitrous oxide, methane and chlorofluorocarbons (Known as Greenhouse Gases, GHGs), contributing to the global warming and consequently producing a negative impact on ecosystems and human life<sup>1</sup>.

Methane, as one of the main GHGs, is of big interest due to its impact in the greenhouse effect. In nature exists a methane cycle with a defined concentration of it in the atmosphere, but nowadays, with the human activities, this cycle is being affected, and methane levels are continuously increasing<sup>2</sup>. This compound is energetically susceptible to be excited with infrared radiation (coming from the sun and reflected by the Earth), which electric field interacts with the fluctuating dipolar moment of methane<sup>3</sup>, increasing the world temperature on a continuous basis due to the formation of a thermal layer in the atmosphere. Furthermore, methane has 25 times the global-warming potential of carbon dioxide (CO<sub>2</sub>) by mass over a century<sup>4</sup>. On the other hand, methane's importance, as a source of energy, is enormous. Its combustion releases<sup>3</sup> 889 KJ/mol and has an availability which has developed a wide variety of technologies based on it. Mainly, it is employed for heating, cooking, and as a fuel for generating electricity for both power industries and households likewise. This compound is the more elemental alkane (CH<sub>4</sub>) with only one carbon atom, that makes it the simplest building block of most bulk organic compounds.

The chemical utilization of methane is a challenge for current technology. Its properties are such that conversion to desired products with high selectivity is difficult: it is relatively inert, it has low electron and proton affinity<sup>5</sup>, low polarizability, weak acidity, high C-H bond strength (415 KJ/mol)<sup>6</sup>, as well as high ionization energy. Furthermore, methane has an extremely high pK<sub>a</sub> (>40) which makes it resistant to attack by most redox active reagents, acids and bases, making the employment of high temperatures or highly reactive reagents a necessary condition<sup>7</sup> for its reactivity.

## **1.2 Valorization of Methane.**

Chemical feedstocks and fuels are fundamental commodities that sustain the life standard of the society; they contribute to the social, economic and technological development of societies that currently relies on fossil fuels<sup>8</sup>. Energy, transportation, and manufacture of goods depend on the majority on oil as a raw material. In the context of a growing world population, the increasing standard living conditions of developing economies countries and the dwindling world oil reserves per capita, a plan to couple an economically favorable with an environmentally friendly solution are unpostponable<sup>9</sup>. Although there are exponential development of alternatives and renewable energy technologies, the interest in improving the current energy obtention from fossil fuels is still valid because most of the mentioned technologies are in a very early stage of growth, hindering its implementation in the short term<sup>8</sup>. Also, the current infrastructure cannot be easily adapted to the newest technologies without big investments and with a total renovation. That is the reason why, in order to implement greener technologies, the efficient use of non-renewable sources is the first step in the transition from fossil fuels to environmentally friendly technologies<sup>10</sup>. Consequently, this highlights the importance of implement new technologies focused on the valorization of methane as an important raw material for energy purposes.

Nowadays, it has been proven the existence of 208 trillion cubic feet methane reserves as natural gas<sup>11</sup>, much more than current oil reserves. The availability of methane, its abundance, and inexpensive acquisition costs, as well as its global dispersion, requires novel chemistry to convert it into easily condensable energy carriers that can be readily integrated into the existing chemical infrastructure<sup>12</sup>. This fact sustains and motivates the research focused on methane exploitation with energy obtention purposes; indeed, environmental sustainability and lower overall costs point to natural gas as the primary source of energy and chemicals in the near future, and methane hydrates as the most important source of hydrocarbons in the long term<sup>9,13</sup>. That is why methane valorization has been a hot topic over the last decades.

Methane is the main constituent of natural gas, it is obtained from biomass activity, as a product of the different anthropogenic processes and as a secondary product in oil

refinement. Also, it is found by tons in clathrates (molecular cages of methane hydrates located in marine substrates in which methane is stored), constituting the largest reserve of not estimated hydrocarbons. Nowadays, the main technology employed to take advantage of this compound is the synthesis gas (a mixture of CO and H<sub>2</sub>) formation and Fischer-Tropsch process, characterized by high energy consumption and the use of large and expensive processing plants. Furthermore, methane can be effortlessly be incorporated into the current petrochemical infrastructure via the conversion to methanol, which is a staple of the petrochemical industry<sup>6</sup>. For that reason, direct conversion processes to obtain methanol and a variety of compounds from methane under mild conditions are unpostponable. In this work, mild conditions refer to cycling processes which work at low temperatures (<500°C) and pressures (preferably 1 atm).

### **1.3 Methanol from Methane, a Fundamental Issue.**

The methane to methanol conversion is of considerable interest in the chemical engineering field. The marked increase of methane availability, as well as its global dispersion, requires new chemistry conditions. The common mechanism of methanol obtention goes directly through a catalytic oxidation process: either via synthesis gas (syngas) and steam reforming or directly into methanol by different processes and technologies. The catalytic production of methanol from methane accomplished through two-step process of high temperature (~1170 K) steam reforming to syngas and its subsequent conversion over Cu-based methanol catalyst, is effective only at large scale<sup>6</sup>. The selective direct methane oxidation forward methanol has a great interest in scientific research for obtaining valuable chemicals directly from natural gas without needing the syngas production<sup>14</sup>. That is, without the employment of huge and expensive infrastructure, high temperatures and pressures; trying to minimize the energy consumption. Methanol, being an intermediate product of the partial oxidation in the complete methane oxidation mechanism, is a desirable and valuable compound to be obtained by low cost and energetically favorable ways. To date, does not exists a catalyst that can convert methane to methanol with high yields and selectivity using oxygen as the sole oxidant in a single step<sup>6</sup>. Methanol, having weaker C-H bonds, is more reactive than methane, leading in facile overoxidation into formic acid and carbon oxides<sup>15</sup>, even at low conversion rates. For that reason, one of the main challenges of this technology is to

control the studied reaction at the specific point of methanol, avoiding methane overoxidation.

Methanol is an important compound to the manufacturing industry, many processes related to the production of high added value products require at any point or stage methanol for work, so methanol is a valuable chemical feedstock. On the other hand, as an energy carrier, methanol offers some advantages compared with methane itself or hydrogen technology, for example. Being liquid at room conditions facilitates its transport and storage increasing safety and lowering risk. Furthermore, the amount of energy liberated in methanol combustion<sup>16</sup> is 726 KJ/mol, more than hydrogen higher heating value. Additionally, methanol as a fuel source that contains a large amount of useful energy which is in high demand to electric energy generation via fuel cell technology applications<sup>17,18</sup>. These advantages have triggered a worldwide quest for new processes, allowing economical small-scale operations at remote locations<sup>12</sup>.

#### **1.4 Methane Monooxygenase.**

In contrast to the harsh process conditions used in many methane oxidative strategies, methanotrophic bacteria convert methane and oxygen into methanol under ambient conditions with remarkable selectivity, through methane monooxygenase enzymes<sup>19</sup>, employing copper and iron as potential active metals<sup>20,21</sup>. These enzymes are a natural catalyst which contains diiron or dicopper centers (soluble methane monooxygenase and particulate methane monooxygenase, respectively) at their active sites<sup>22</sup>, which catalyze the hydroxylation of methane to methanol using atmospheric O<sub>2</sub>, through the use of NADH (Nicotinamide adenine dinucleotide) as a reducing agent<sup>23</sup> to the activation of oxygen, with high selectivity and effectiveness ( yields near 100%). In soluble methane monooxygenase, the active site of the hydroxylase contains bis( $\mu$ -oxo)diiron core<sup>23</sup>, while in particulate methane monooxygenase the active site contains a copper cluster that catalyzes the insertion of oxygen into the methane C-H bond<sup>24</sup>. The proper ligand field environment stabilized in the metalloenzyme structure afforded by copper and iron ions generates electrophilic metal-oxygen species capable of attacking the strong C-H bonds of methane<sup>6</sup>. In terms of the catalytic activity per active site, enzymatic systems are dramatically more efficient than the current catalyst used in today's industrial reactors.

In order to optimize the conversion activity, efforts have been done focused in reproduce the methane monooxygenase active sites in synthesized catalysts. Many research groups have studied new materials which can emulate the methane monooxygenase activity using first-row transition metals (copper, iron, and cobalt)<sup>25-27</sup>; between them, metal ion-exchanged zeolites as the ones used in this work, particularly, copper exchanged mordenites.

### 1.5 Current Technologies to Obtain Methanol from Methane.

Nowadays exists different studied pathways for methane to methanol conversion with varying availability and methanol yields. All of them share a main aim: to control the conversion reaction to the specific point of methanol employing mild conditions and maximizing the methanol yields. The following figure shows a scheme of the currently available technologies for the methane oxidation process. This work is enclosed in the field of Low-Temperature Heterogeneous Catalysis.

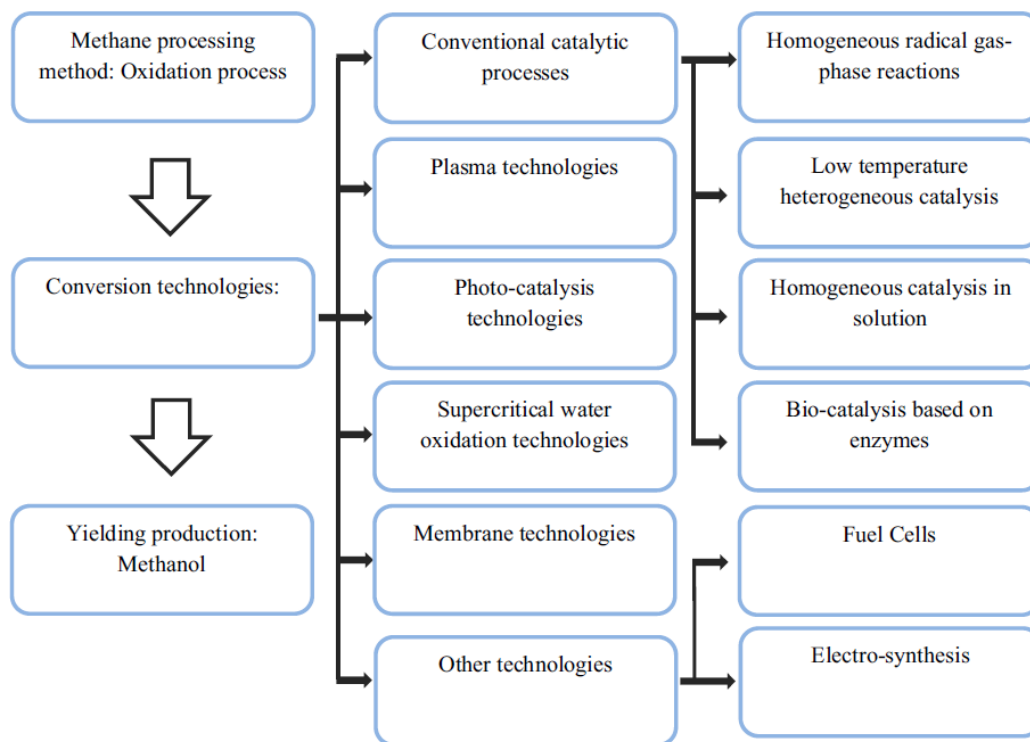


Figure 1.1.5.1. Conversion Pathways of methane to methanol, scheme taken from the work of Zakaria, Z. et al. 2017

### 1.5.1 Direct conversion of methane to methanol via conventional catalytic processes.

The catalytic conversion of methane to methanol is basically a partial oxidation process and could be described by the following equation<sup>18</sup>:



The reaction can be carried on in liquid and gas phases. And the commonly used parameters lay between 30-200 bars of methane atmosphere and 200°C to 700°C<sup>18,28</sup>. The first step in the mechanism is the activation of the C-H bonding of methane. The second step is the splitting of the covalent bonding through electrophilic attack to yield e<sup>+</sup>-CH<sub>3</sub>, producing the oxidized products from methane.

### 1.5.2 Homogeneous Radical Gas-Phase Reactions.

In this technology, the gas-phase reaction occurs due to a free radical mechanism at high pressure and temperature<sup>29</sup>. The methane is the rate-limiting step due to the formation of methyl radicals and, as a consequence, a variety of materials are employed to reduce the energy barrier of hydrogen abstraction<sup>30</sup>. As fundamental variables to optimize the yields in this technology are the temperature and the pressure. Holmen reports the best condition for the gas phase reaction: temperatures 450°C-500°C, and pressures of 30-60 bars; reaching 30-40% of methanol yields and 5-10% of methane conversion<sup>31</sup>. The design of the reactor systems is a significant field of study with the objective of maximize the yields, as summarize Zakaria *et al.* A disadvantage of this gas-phase route is the low control of selectivity and the costs (monetary and energetically speaking) of high operating pressure.

### 1.5.3 Heterogeneous Catalysis at Mild Conditions.

In this technology, there are applied low pressures (1-10 bars) and temperatures; for that reason, the design and the selection of the catalysts are crucial to increase the yields. The catalyst (solid) and the methane (gaseous) are in different aggregation physical state. Many catalysts have concerning the efforts to optimizing its catalytic performance with a slightly reduced state by storing the isolated metal oxide on a silica substrate<sup>18,29</sup>. A variety of metal insertions have been tested in different matrices with the purpose of increment the methanol yields<sup>18,22</sup>, at the same time it has been proposed mathematical models and theoretical studies shedding light about the nature of the active sites<sup>32</sup>. Between them, Tabata *et al.* propose the H-abstraction of methane molecule by reduction of molybdenum

and vanadium to  $\text{MoO}_2$  and  $\text{V}_2\text{O}_3$ , respectively<sup>30</sup>. Zhang tested perovskite-type oxides based in lanthanum cobalt oxides, founding good activity in the methane oxidation with a vertical flow fixed bed reactor<sup>33</sup>. The catalytic activity of phthalocyanine complexes of iron and copper located in zeolite (Pentasil and Y) frameworks were tested with different oxidants ( $\text{O}_2$ /tert-butyl hydroperoxide) obtaining the highest yield activity and conversion reported so far<sup>34</sup>. Ionic exchanged zeolites have been proved, particularly, many studies have been focused in metal (Iron, Cobalt, and Copper) exchanged Zeolony Mobil Oil-5 (ZMS-5) producing promising results that can be improved through synthesis methods and reactors design<sup>35-37</sup>.

The direct methane to methanol conversion at mild conditions via heterogeneous catalytic partial oxidation is a promising alternative to the current methods of massive methanol production, leading to a decrease in the market cost of methanol and many derived from it<sup>18</sup>. This technology requires lower energy consumption and can be carried out under ambient conditions<sup>18</sup>. Unfortunately, a heterogeneous catalysis technology that can carry out the methane to methanol conversion with good efficiency and selectivity, and potentially to be inserted in the industry, has not been proposed<sup>38</sup>. The conversion ratio of methanol produced with this technology is not sufficiently high to provide a new energy system; it is needed more information, and more research focused on this aim.

#### *1.5.4 Homogeneous Catalysis in Solution.*

As the category indicates, both the catalyst and the methane, are maintained in a solution, and the reaction occurs in the same solution. In this field, Periana *et al.* developed Platinum(II), Palladium(II) and Mercury(II) based catalysts, such as bipyrimidyl platinum complex, with significant results<sup>39,40</sup>. Shilov *et al.* tested with Palladium(II) and Palladium(IV)<sup>41</sup> with good methanol yields results. Zeolites have been employed through this technology, particularly Fe-ZSM-5, Co-ZSM-5<sup>25</sup>, and Cu-ZSM-5 catalysts, with the highest methanol and formaldehyde yields<sup>42</sup>, with methanol selectivity for Cu-ZSM-5<sup>43</sup>.

The methane to methanol conversion using low temperature in solution can achieve higher yield by controlling the operating parameters like temperature, methane/oxygen ratio,  $\text{OH}^-$  concentration, and residence time<sup>18,30</sup>. In the case of temperature, it has been studied in the range from  $35^\circ\text{C}$  to  $700^\circ\text{C}$ , with a better performance at  $100^\circ\text{C}$ <sup>44</sup>.

#### *1.5.5 Bio-Catalysis Based on Enzymes.*

The main feature of this technology is the mimicry of the specific active sites found in pMMO (particulate methane monooxygenase) and sMMO (soluble methane monooxygenase), and the employment of methanotrophs with controlled conditions to produce methanol. Razumovsky *et al.* explored biocatalyst based on the cell of the bacteria *Methylosinus Sporium B-2121* for converting methane to methanol through biochemical formation<sup>18,45</sup> processes. Other studies, focused in the production of formaldehyde and methanol from exchanged zeolites in contact with methane, and molecular oxygen as oxidant agent, in an attempt to mimic the natural active sites in pMMO and sMMO in zeolites framework<sup>46</sup>.

#### *1.5.6 Plasma Technologies.*

Plasma is referred to the fourth state of matter, and it includes several components: positive ions, negative ions, electrons, and neutral species. This technology is related to the methane oxidation towards methanol in a plasma medium, varying some reaction conditions like pressure and temperature. Also, this technique offers a clean destruction of hazardous waste and no harmful emission of toxic waste such as CO<sub>2</sub> and CO. Thermal plasma and non-thermal plasma are employed in the oxidative decomposition of methane. Complete reactor design is needed for the production of significant quantities of methanol with plasma technologies<sup>18</sup>.

#### *1.5.7 Photo-Catalysis Technologies.*

The base of this photo-catalytic technology is a photochemical reaction that is carried out with external energy provided by ultraviolet light radiation that has energy equal or greater than the energy band gap of the used materials (e.g., semiconductor). This technique is an old probed option for methane conversion and classified as a green alternative for selective oxidation. The main requirements for this method are light, water and methane (abundant and inexpensive). Many catalysts have been designed and developed for photocatalytic reactions, however low yields of methanol are still obtained; difficulting its transition to industrial scaling<sup>47</sup>.

### *1.5.8 Supercritical Water Technologies.*

Also known as hydrothermal oxidation, this technique provides a high-efficiency conversion and thermal oxidation process to treat a wide variety of hazardous and non-hazardous wastes. The studies focused on methane oxidation to produce methanol with this technology are still limited due to problems associated with reactor design, the high temperatures needed, and the high corrosion rate when treating wastes containing halogens<sup>18,48</sup>.

### *1.5.9 Biological Technology (Membranes).*

This technology allows the methane to methanol conversion via a biological process based on membrane reactor technology. The membranes can separate a material physically and serve as a reactor for methanol conversion, so, it has a dual function. These materials can be classified in function of its composition and its porosity. Commonly, for methane to methanol conversion are used inorganic membranes with added transition metals or ceramic materials, resulting in great physicochemical stability<sup>48</sup>.

### *1.5.10 Other Technologies for Methane to Methanol Conversion.*

The employment of fuel cell type reactors enables the methane oxidation with increased selectivity to methanol. It is needed a catalyst (usually based on transition metal oxides), a cathode and an anode. Many catalysts have been tested, such as various metals (Pd, Ru, Au, Ag) and metal oxides ( $V_2O_5$ ,  $F_2O_3$ ,  $CoO$ ,  $Mn_2O_3$ ,  $MoO_3$ ,  $CrO$ ) supported by a mesh (e.g., stainless mesh) with optimized results. The temperatures range employed with this technology are from 50°C to 250°C<sup>49</sup>.

The electrosynthesis via gas diffusion electrodes (GDEs) is another technology for methane oxidation via electrochemical cell. The advantage of this technique is the ability to tune a required electric potential to optimize the production of methanol. On the other hand, a disadvantage is the formation of by-products such as formic acid and formaldehyde during the methane oxidation<sup>50</sup>.

## 1.6 Copper-Mordenite Based Technologies.

It is reported that the most promised C-H activation catalyst candidate thus far is Cu-based zeolites, where  $\text{Cu}^{\text{III}}\text{-O-Cu}^{\text{III}}$  site is believed to be the key active site for the selective oxidation of methane to methanol accordingly with theoretical studies<sup>6,32</sup>. These sites operate stoichiometrically<sup>43,51</sup> and catalytically<sup>52</sup>. These materials have great potential in methane to methanol conversion; however, they still produce reduced amounts of methanol. High methanol selectivities could only be achieved at very low conversions (<0.1%)<sup>6</sup>. Indeed, theoretical studies predict that overoxidation of methanol into  $\text{CO}_2$  and  $\text{H}_2\text{O}$  at isolated  $\text{Cu}^{2+}$  sites will proceed extensively at methane conversion above 0.2%<sup>6,53</sup>.

The MMO metalloenzymes, as a natural process, use a combination of effects that are difficult to replicate using inorganic catalysts. Accordingly with K. T. Dinh *et al*, the main necessary features to get a material with high selective methanol production are: “(1) ligand fields that induces high-spin electronic configurations at the transition metal sites, which induce highly reactive oxidative and reductive environments, and (2) a complex gating mechanism that influences the lability and dynamic binding of reagents to the active sites, which enables methanol transport out of the active site pocket while also forbids back diffusion”<sup>54</sup>.

Zeolites, and specifically Mordenite, share many of the attributes related with the isolation and ligand field strength observed in the metalloenzymes<sup>6</sup>, and works to produce methanol from methane, but, according to the results reported so far, everything indicates that we are still far from finding an industrially viable catalyst for this direct methane to methanol conversion.

### 1.6.1 Zeolite Framework: Mordenite.

As mentioned before, the present work belongs to the low-temperature heterogeneous catalysis group<sup>18</sup> of the conventional catalytic process. Following this research line, different materials have been tested towards the methane to methanol conversion, between them zeolites are broadly studied<sup>7,14,19,51,55–58</sup>. Particularly, mordenite exchanged with transition metals (e.g., copper<sup>7,32,58</sup>, iron<sup>59</sup>, and cobalt<sup>25</sup>) show an important activity in the methane to methanol conversion because the mordenite framework can stabilize the metal ions forming specific active sites through the formation of metal oxides in a similar

configuration as reported in metalloenzymes<sup>60</sup> (MMOs and MMOp). Mordenites also have an open porous framework and a large surface area, structural features that favor the transit and interaction of chemical species inside it<sup>61</sup>.

Mordenites are a common group of zeolites with the chemical formula<sup>61</sup>  $(Ca, Na_2, K_2)Al_2Si_{10}O_{24} \cdot 7H_2O$ . It is one of the most abundant zeolites used commercially. We cannot find them as pure compound because the mordenite framework has a negative charge that must be compensated with ionic species (cations) at specific sites neutralizing the whole structure. Precisely, ionic exchange refers to the substitution of one kind of ion present in mordenite by another provided by a metal precursor. Mordenite crystallizes with an orthorhombic unit cell in the  $Cmcm$  space group with cell parameters<sup>62</sup>  $a=18.13$ ,  $b=20.5$ ,  $c=7.52$  Å. Its porous framework is constituted by parallel 12-membered (aperture  $7 \times 6.5$  Å), and 8-membered (aperture  $5.7 \times 2.6$  Å) rings channels which can communicate between them by a less compressed 8-membered rings channels ( $3.4 \times 4.8$  Å)<sup>62</sup>.

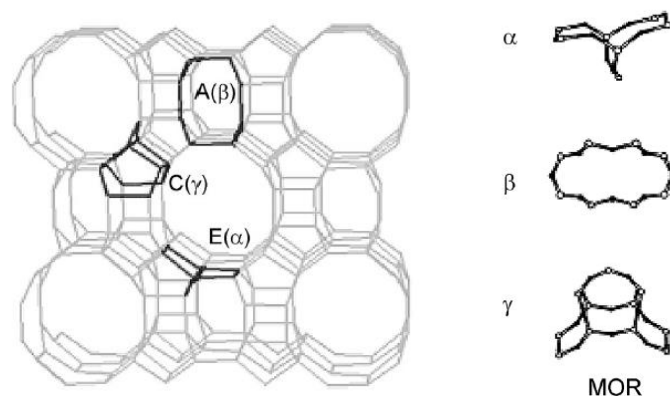


Figure 1.6.1. Mordenite Structure with crystallographic sites  $E(\alpha)$ ,  $A(\beta)$ , and  $C(\gamma)$  indicated in black (Vanelderen, et al. 2014).

Copper Mordenite is appreciated due to its catalytic potential; this is not only because the uniformity of copper species but also owing to its high concentration of active copper sites resulting in an unprecedented activity of the material. It is mainly used for nitrogen oxides ( $NO_x$ ) decomposition<sup>63</sup> and, in the petrochemical industry, as a catalyst for the obtention of high value-added products<sup>64</sup>. Recently, some years before, Copper (II) exchanged mordenite has been employed in the methane conversion at low temperatures<sup>7,10,18,55,56</sup>.

Mordenite is chosen to produce copper clusters because it is known that its framework allows a preferential exchange of the sites located in the constrained side pockets<sup>65</sup>.

### **1.6.2 Reported Synthesis of Copper Exchanged Mordenites.**

The ionic exchange process is probably the most widely used route to modify zeolites properties. Two usual methods for synthesizing copper mordenites are by aqueous solution<sup>51</sup> and by solid-state ion exchange<sup>58</sup>. The aqueous solution synthesis pathway for cluster formation in mordenite framework is associated with two requirements: (i) the exchanging species must be well defined in the aqueous solution, and the precipitation of the metal cation by changes in the pH during the exchange procedure has to be avoided; (ii) the exchanged cations need to form a defined thermodynamically stable configuration upon coordination to the zeolite lattice<sup>12</sup>. The second requirement is also necessary for the solid state synthesis; this method has demonstrated indeed a higher degree of ion exchange<sup>58</sup>. The ionic exchange under milling facilitates the cation entrance to the mordenite framework because the hydration effect on the effective ion size is minimized, enabling its diffusion through the material porous framework<sup>66</sup>. Also, in solid-state synthesis, the exchange process occurs far away from the equilibrium, causing the microcrystals to collide and liberate localized energy leading to hot points where local phase transitions, the occurrence of redox reactions, and formation of solid solutions and metastable phases are possible<sup>67</sup>. In addition, Reguera *et al.*, reported that the particles fractured under milling conditions induces the solid activation through the appearance of structural defects and active sites. However, for the solid-state ionic exchange, all these features and their effects have not been reported at all.

The milling process can be done with an Agata mortar<sup>68</sup> or preferentially with a system, as a ball mill, that can homogenize the applied force, and therefore the energy supplied into the system. The amount of NH<sub>4</sub>-Mordenite and the copper precursor are in function of the copper loaded percent desired by stoichiometric calculus<sup>68</sup> and the amount of material produced is limited by the dimensions of the ball mill grinding vessel.

After the milling process, comes an activation stage that consists of calcination in the presence of oxygen<sup>55,56,68-70</sup> (e.g., the air, NO, or O<sub>2</sub> atmospheres). The calcination temperatures range starts from 150°C<sup>19</sup> to 700°C<sup>58</sup> to be considered as a mild conditions

process; always at lower temperatures than that applied in conventional methanol production by syngas and catalytic steps. At this stage of the process occurs the ionic exchange between the copper and the previously ionic-bonded cation (e.g., Na, NH<sub>4</sub>); also, the elimination of the copper precursor residues occurs, leaving exclusively the copper ions inserted in the zeolite framework<sup>53</sup>. The temperature activation is also necessary for the dehydration of the materials and the induced migration of the exchanged copper ions towards the formation of the copper oxide cluster<sup>12</sup>. From here on, the material can be tested in the methane to methanol reaction.

### **1.6.3 Active sites in Copper Mordenite for Methane to Methanol Conversion.**

Copper exchanged mordenite (Cu-Mordenite) has demonstrated good performance for methane conversion, specifically towards methanol<sup>51,55,56</sup>. To synthesize this material, a neutral mordenite (e.g., Na-Mordenite<sup>58</sup> and NH<sub>4</sub>-Mordenite<sup>68</sup>) is employed as a matrix, commonly coming from commercial origin. As ion copper precursor, a variety of materials like copper (II) acetylacetonate<sup>68</sup>, copper (I) nitrate<sup>58</sup>, copper (II) acetate<sup>71</sup>, copper (II) chloride<sup>51</sup>, etc., have been used; where it is chosen one of the previous precursors in dependence of the oxidation state of the copper ion to be inserted, the specific desired sites to be formed in the mordenite framework and the synthesis route to be followed. Usually, Cu-Mordenite is proved in flow reaction systems with a cycled operation mode in which the spectroscopical analysis are done *in operando*<sup>7,19,55</sup>. Another reported experimental procedure consists of the employment of a Batch reaction system characterized by static atmosphere conditions.

The quantity of copper exchanged material depends on the Silicon/Aluminum ratio, the oxidation number of the copper ion given by the precursor, and the synthesis route employed. For example, if the Si/Al rate changes, the total electric charge of the mordenite framework is different, changing indeed, the population of ions needed to neutralize its structure. Different copper precursors provide its metal ions with major or minor efficiency and it also depends on the interaction with the mordenite and the synthesis pathway employed. The oxidation state is relevant because, as a function of this number, it is possible to insert more or less copper ions; this is because the mordenite framework

has a well-defined charge that must be neutralized in the ionic exchange process; for this reason, it is possible to exchange more copper (I) than copper (II) in the same material.

The possibilities of active copper sites formed in a mordenite exchanged material have been broadly studied; but, even so, there is no consensus on the exact structure of the active copper site nor its mechanism for methane transformation. For this reason, mononuclear<sup>53</sup>, binuclear<sup>43</sup>, and trinuclear<sup>12</sup> proposal exists, based in Density Functional Theory (DFT) and Quantum Mechanics/Molecular Mechanics, that explains the process. In the case of copper exchanged zeolites, reactivity has been ascribed mainly to  $\mu$ -oxo dicopper sites, and more recently to a tricopper site.

The principal reported site, as responsible to the methane to methanol conversion, in Mordenite and ZSM-5 exchanged with copper ions, is the mono( $\mu$ -oxo) dicopper(II) species<sup>19,28,55,58,70,72,73</sup> ( $[\text{Cu}_2(\mu\text{-O})]^{2+}$ ), which is mainly identified by electronic spectroscopy with the formation of a broad band near the  $22200\text{ cm}^{-1}$  region<sup>19,74</sup> for mordenites and  $22700\text{ cm}^{-1}$  region<sup>19,70,74</sup> for ZSM-5. This signals are interpreted as a charge transfer  $\text{O}_{\text{bridge}} \rightarrow \text{Cu}$  transition on samples heated in the presence of oxygen's air<sup>58</sup>. It appears when the calcination temperature ranges come from  $280^\circ\text{C}$  to  $700^\circ\text{C}$  in the presence of  $\text{O}_2$  and/or  $\text{NO}_2$  atmosphere<sup>28</sup>. This band tend to disappear in the presence of methane<sup>68</sup>; suggesting that a dinuclear Copper core is responsible for the activity towards

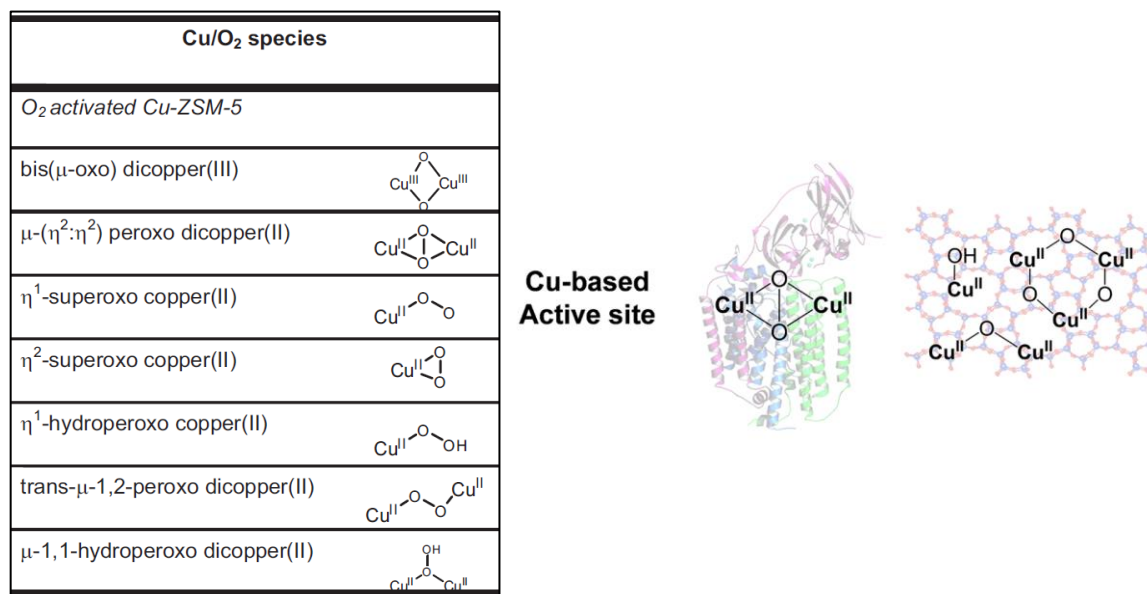


Figure 1.6.2. Left: Spectroscopically characterized mononuclear and binuclear Cu/O<sub>2</sub> species (Woertnik, et al., 2009). Right: current active site motifs for Cu-based enzymes and zeolites (Dinh, et al., 2018).

the selective oxidation of methane to methanol. As a probable position of this species is the  $\beta$  channel in mordenite framework<sup>58</sup>, the dicopper core is probably occupying two neighboring extra-framework positions for the exchanged metal<sup>73</sup>.

Different species reported for ZSM-5 are shown in figure 1.6.2, according to Woertnik *et al.* work. In the case of mordenite species, there is no consensus in the species found, and the question about nature of the possible active sites is still open<sup>6</sup>. The figure shows the most probable active site motifs for Cu-based enzymes and zeolites, accordingly to Dinh *et al.* work.

Chan *et al.*, proposed a cluster in pMMO of tricopper complexes for selective methane oxidation to methanol that employs H<sub>2</sub>O<sub>2</sub> as oxidant agent<sup>75</sup>. A few years ago, Sebastian Grundner *et al.* reported a tricopper species (trimeric site) as responsible for methane oxidation to methanol in the mordenite framework. Furthermore, selective stabilization of a single-site Cu-oxo clusters in mordenites is possible for the trimeric<sup>12,76</sup> species [Cu<sub>3</sub>( $\mu$ -O)<sub>3</sub>]<sup>2+</sup>, reaching not only the uniformity of this Copper species but also a high concentration of this sites, resulting in an unprecedented activity of Copper exchanged mordenite in methane oxidation<sup>12,77</sup>. The proposed stoichiometry suggests a formal mixed Cu(II)/Cu(III) composition of the cluster<sup>12,32</sup>. The complex line shape insinuates at least two types of oxygen donor ligands with significantly different Cu-O distances due to the framework and the extraframework oxygen. Aluminum framework atoms in the 8-membered ring side pockets of H-Mordenite provide the conditions to stabilize the [Cu<sub>3</sub>( $\mu$ -O)<sub>3</sub>]<sup>2+</sup> sites<sup>77</sup>. This experimental data deviate from the spectrum bands assigned to the binuclear complex ([Cu<sub>2</sub>( $\mu$ -O)]<sup>2+</sup>); the reported ultraviolet-visible spectroscopy band for the trimeric site is centered<sup>12</sup> at 31000 cm<sup>-1</sup>. This band is stable at 200°C under O<sub>2</sub> flow, disappearing in contact with methane flow at 200°C.

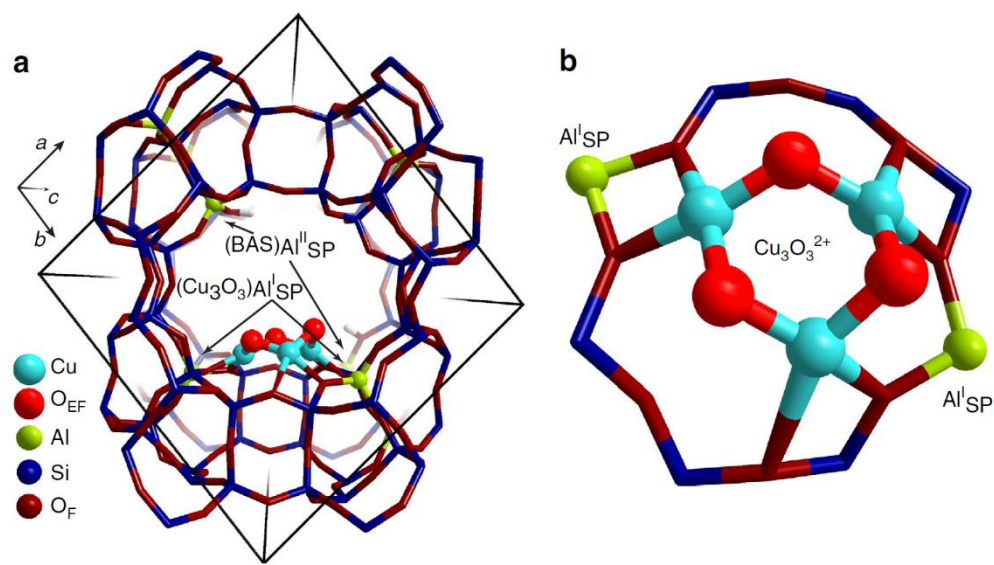


Figure 1.6.3. Structure and location of  $[\text{Cu}_3(\mu\text{-O})_3]^{2+}$  cluster in mordenite predicted by DFT, reported by Sebastian Grundner et al.

#### 1.6.4 Methane to Methanol Conversion Process.

Methane activation occurs in the active site by homolytic cleavage of C-H bonds by a radical, like oxygen, to form a radical methyl intermediate that is subsequently converted to hydroxyl species<sup>32,73,76</sup>. Consequently, the methanol keeps adsorbed into a reduced Copper cluster waiting to be removed by another agent. In the case of trimeric species, the C-H bond activation occurs over the extra-framework  $\text{Cu}_3\text{O}_3^{2+}$  through a formally radical-anionic extra-framework oxygen centre<sup>12</sup>. The interaction results in the cleavage of the C-H bond, resulting in  $\text{CH}_3\cdot$  radical and an OH group bound to the cluster<sup>12</sup>. The main purpose of copper centers in the active site is to stabilize the electronic configuration of the extra-framework cluster with the anion-radical character of the oxygen ligands crucial for the C-H activation<sup>78</sup>. The next step of this process is the recombination of the  $\text{CH}_3\cdot$  radical with the copper cluster bounded to the OH group, producing the so-formed methanol adsorbed into the copper cluster, coordinated to two neighboring copper centres<sup>12</sup>.

#### 1.6.5 Methanol Desorption Process and Regeneration of Activated Material.

The usual desorption process of the methanol contained into the zeolitic framework is by a steam treatment at different temperatures, in which copper clusters are hydrolyzed

liberating the methanol adsorbed<sup>7,19,55,68</sup>. Other studies have reported the methanol desorption with liquid water at room temperature<sup>68</sup>. It is possible to reactivate the material once the methanol has been desorbed, by the same calcination process discussed in Method of Synthesis of Copper Exchanged Mordenite section<sup>56,68</sup>, and employing it in another reaction cycle to produce methanol again. The yields in the consecutive reaction cycles are approximately maintained after four cycles<sup>55,68</sup>.

## **1.7 Analytical Techniques Employed to study the Methane to Methanol Conversion by Copper (II) Exchanged Mordenites.**

### *1.7.1 Ultraviolet-Visible Spectroscopy.*

Ultraviolet-visible (UV-Vis) spectroscopy is a technique that provides information about the electronic behavior of materials. It works by means of the interaction between a part of the ultraviolet radiation and the full adjacent visible spectral regions with matter. The phenomena produced in this interaction are associated with the electronic energy transitions, occurring by absorption of photons. In general, the physical principle of this phenomena is related to the promotion of an electron from its ground state to an excited state due to the absorption of UV-Vis radiation. Usually, the UV-Vis light is absorbed by valence electrons, that is taken to an empty excited state (higher energy). The differences in energy vary according to the nature of the orbitals. Molecules containing bonding and non-bonding electrons can absorb energy in the UV-Vis range, producing four types of transitions:  $\pi \rightarrow \pi^*$ ,  $n \rightarrow \pi^*$ ,  $\sigma \rightarrow \sigma^*$  and  $n \rightarrow \sigma^*$ <sup>79</sup>. The physical principle of this technique is described by the Lambert-Beer's law:

$$A = \log_{10} \left( \frac{I_0}{I} \right) = \epsilon c L$$

Where A is the measured absorbance,  $I_0$  is the incident light; I is the transmitted light, L is the path length through the sample, c is the concentration of the absorbing species and  $\epsilon$  is the extinction coefficient<sup>79</sup>.

To study catalysts, it is usual to employ the UV-Vis diffuse reflectance spectroscopy. This technique is used when the materials are weak absorbents to the wavelength employed and when the light penetration is high enough with respect to the applied wavelength. For

copper exchanged mordenites is convenient to make use of the Kubelka Munk function to detect the nature of the species under study<sup>7</sup> (See Anexus 7).

### *1.7.2 Infrared Spectroscopy.*

Infrared (IR) spectroscopy is an analytical technique that involves the interaction between infrared electromagnetic radiation with matter. It usually works on the base of the absorption of IR radiation phenomena by molecules, producing an IR absorption spectrum; but, emission and reflection are other possible configurations of IR analysis sustained in the absorption of energy, causing a transition to a higher energy level of rotational, vibrational, or electronic possibilities. It's important to state that the energy is quantized and absorption of radiation causes a molecule to move to a higher internal energy level. For a molecule to be IR active, there must be a change in dipole moment as a result of the vibration that occurs when IR radiation is absorbed. The absorption of IR radiation occurs when the alternating electric field of the radiation interacts with the molecule, causing a change in the molecule movements. There exist multiple possibilities of movements for the different possible energy levels for the three types of transitions<sup>80</sup>.

IR spectroscopy is very helpful to identify the species and groups belonging to a molecule and to follow the possible changes in each step of a process in which the same molecule, group or species is involved<sup>81</sup>.

### *1.7.3 Electron Paramagnetic Resonance.*

Electron Paramagnetic Resonance (EPR) is an analytical technique that take advantage of the quantum properties of electrons. By inciting a stablished monochromatic electromagnetic radiation on a sample that is inside a variable magnetic field, it is possible to induce a Zeeman effect in paramagnetic species producing spin transitions, in other words, EPR is concerned with the splitting of electronic spin states. EPR probes the interaction of magnetic dipoles with an applied magnetic field and electromagnetic radiation of appropriate wavelength. Paramagnetic species are those who has unpaired electrons; from them arises the electron magnetic dipole. According to the nature of spin paramagnetic species different transitions can be seen at different magnetic field values owing to different phenomena that occurs in the nucleus-electron system. The g-value can be used as an identifier for a given paramagnetic species, however, note that g-value

designate the intrinsic resonance position of a radical in a particular environment rather than being given relative to a reference compound<sup>82</sup>. Since the unpaired electron is typically bound to a molecule, the g-value for a given paramagnet usually deviates from  $g_e$  (the free electron g-value,  $g \sim 2.0023$ ). The magnitude of the shift depends on the molecular environment and ultimately the spin-orbit interaction. According to the material  $g$  can be isotropic, axial or rhombic. EPR spectrum may be broadened due to  $g$  anisotropy<sup>83</sup>.

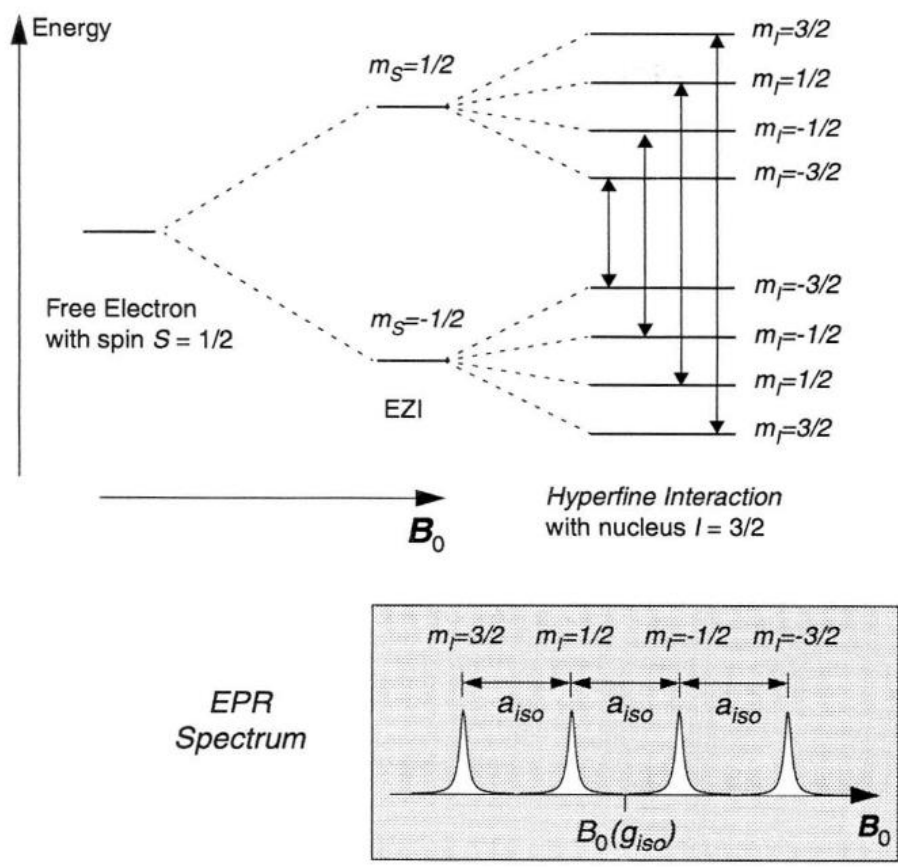


Figure 1.7.1. Energy level diagram and resulting EPR spectrum for a spin system with one electron  $S=1/2$  and a nucleus  $I=3/2$ , picture taken Schosseler work.

The physical description of EPR is resumed by the relation  $E = m_s g_e \mu_B B_0$ , where  $B_0$  is the magnetic field applied,  $\mu_B$  is the Bohr Magneton,  $g_e$  is the electron g-factor,  $m_s$  are the spin quantum number magnetic components and  $E$  correspond with the energy between spin states. According to the Zeeman effect, when a magnetic field  $B$  is present the degeneracy of spin states is broken and the difference in energy of a system with  $S=1/2$  is

given by the relation  $E = g_e \mu_B B_0$ . But, EPR can offer more information because it is sensible to the hyperfine interaction. The interaction of the electron spin with a nuclear magnetic moment is called hyperfine interaction. In figure 1.7.1 the effect of the hyperfine coupling on the energy level diagram and the EPR spectrum is illustrated for the simple case of isotropic electrons Zeeman interaction and hyperfine interaction for a spin  $I=3/2$  (e.g.  $\text{Cu}^{2+}$ ). The coupling between the electron and nuclear spin results in a splitting of each electron spin state into 4 levels. The allowed transitions obey the selection rules  $\Delta m_s = \pm 1$  and  $\Delta m_I = 0$ , and are shown in the energy level diagram. The resulting EPR spectrum consists of four lines centered about  $g_{\text{iso}}$  and  $a_{\text{iso}}$ <sup>84</sup>.

#### *1.7.4 X-Ray Diffraction.*

X-Ray Diffraction technique is specifically employed to determine the atomic and molecular structure of materials. This technique works inciting an X-Ray beam on a sample that diffracts the beam into many specific directions on a plane and analyzing the diffracted beams in a determined angular range. It is based in the physical principle of diffraction produced by crystalline materials and described by the Bragg's law. X-Ray is used to produce the diffraction pattern because their wavelength is typically of the same order of magnitude as the spacing between the planes in the crystal<sup>85</sup>.

In the case of copper exchanged mordenites, this technique helps to determine the changes in the mordenite structure when the copper ion is exchanged. Also, it gives information about the size of the copper nanoparticles if any, and information about the homogeneity of the samples<sup>68</sup>.

#### *1.7.5 Gas Chromatography-Mass Spectrometry.*

Gas Chromatography-Mass Spectrometry (GC-MS) is an analytical technique that is employed to identify and quantify different species within a test sample. The functioning of GC-MS lies in the separation of the molecular components of a solution through a large column (capillary or packed) in which circulate an inert gas (mobile phase). As a function of the mass and the physical interaction that occurs inside the column, between the components and the column coating, each of the components of the initial solution will have a specific time of retention, leaving the column separately, being analyzed by Gas Chromatography detectors (e.g., Flame Ionization Detector, Thermal Conductivity

Detector, etc), and moving to the mass spectrometry system. Separately, mass spectrometry (MS) is an analytical technique that measures the mass-to-charge ratio of ions; this is useful because once the separated components enter to the MS system, they are bombarded with electrons in order to break the molecules, producing charged and separated fragments according to the mass-to-charge ratio. In this case, when it is applied an electric field, ions of the same mass-to-charge ratio will undergo the same amount of deflection and will be identified.

In methane to methanol conversion by copper exchanged mordenites, this technique is employed to identify if the methanol is obtained after the conversion process, if the no desired species were formed, and quantify all of them in order to obtain the yields and selectivity of materials towards methanol<sup>58,68</sup>.

#### *1.7.6 Adsorption Analysis.*

The gas adsorption technique is used to measure the specific surface area and pore size distribution of porous materials. The dry sample is degassed and cooled at a temperature of 77 K (liquid nitrogen)<sup>86</sup>. At this temperature, nitrogen is physically absorbed on the surface of the sample. An adsorption isotherm (at a defined temperature) is usually recorded as the volume of gas adsorbed as a function of pressure. Using relative pressure to construct the isotherms eliminates the changes in pressure from small changes in temperature. Normally, a small change in the temperature modifies the saturation vapor pressure remarkably. The absorption process can be considered to be a reversible condensation or layering of molecules on the sample surface during the heating is evolved<sup>87</sup>. For copper exchanged mordenites, Nitrogen, whose kinetic diameter is 3.6Å<sup>86</sup>, is an ideal molecule to measure its surface area and pore size distribution<sup>68</sup>.

The physical adsorption of gas molecules on a solid surface studied with BET Theory (Brauner-Emmet-Teller Theory) serves as the basis for an analysis technique which allows the measurement of the specific surface of porous materials. T-plot analysis<sup>88</sup> gives information about the volume and the mean porous size. And with BJH (Barret-Joyner-Halenda Theory) adsorption-desorption model, it is possible to construct a distribution of porous volumes to define the porous physical properties<sup>58,87</sup> of the material.

### *1.7.7 Thermogravimetric Analysis.*

This thermal technique measures the changes in a defined mass of a sample over time as the temperature changes. The information provided is related to different phenomena, such as phase transitions, adsorption, desorption, thermal decomposition, and solid-gas reactions.

For copper exchanged mordenites, this technique measures the mass loss during the calcination process. It is possible to determine the temperatures in which the copper precursor is eliminated, leaving only the copper ions, and the moving of chemisorbed and physisorbed water molecules; complementing the degassed temperatures needed for other studies<sup>58</sup>.

### *1.7.8 Scanning Electron Microscopy (SEM)-Electron Dispersive X-Ray Spectroscopy (EDS).*

We employed the scanning electron microscopy to analyze the changes that copper insertion produces in the morphology at a certain (micrometer) level but it is not possible to see the incorporated metal sites because its dimensions are below to the detection limit of this technique<sup>81</sup>. SEM works by scanning a surface with a focused beam of electrons. These electrons interact with the atoms in the sample surface producing different signals that can show us information about the surface topography and composition of the sample. Energy dispersive X-ray spectroscopy is an analytical technique used for the elemental analysis or chemical characterization of a sample. This technique is based on the emitted X-ray when the electron beam removes an inner shell electron from an atom of the sample causing a higher energy electron to fill the shell and release energy.

## 2. EXPERIMENTAL SECTION.

In literature, it is common to find two main synthesis routes to obtain metal ion exchanged materials. Typically, the synthesis pathway employed is by using an aqueous solution or *via* liquid phase ion exchange. Nowadays, solid-state ion exchange has gained interest since Bozbag *et al.* performed a solid-state ion exchange between H-mordenite with copper (I) chloride<sup>51</sup>. Reguera *et al.* and Parishan *et al.* have already proved this solid-state synthesis route with excellent results in the metal ions exchange degree<sup>58,68</sup>. The solid-state reaction facilitates the metal ion diffusion through the mordenite empty channels and the accessibility to available sites for the exchangeable charge-balancing cation in the material framework.

Another issue to consider in the synthesis pathway is the desired homogeneity of active sites in the mordenite framework. A desirable feature in this kind of materials is the obtaining of a unique type of active sites which may facilitate their study and characterization. In this section, we present a synthesis method of copper exchanged mordenite materials that apparently produce the trimeric copper-oxo cluster, a species previously reported by Grundner *et al.*<sup>12,32,89</sup>.

### 2.1. Experimental Design.

We designed and applied a complete 2<sup>k</sup> experimental design with three variables. We chose the experimental variables of study according to the available laboratory conditions: Activation temperature, copper loaded weight percent and methane pressure in the reaction. Table 2.1.1 shows the design and description of the variables.

*Table 2.1.1. Experimental Design and Description of variables. According to the notation employed in the experimental design, the assignment -1 refers to the lower value of each variable (300°C, 1% wt Cu, 2 bar), the assignment 0 refers to the central points (400°C, 3% wt Cu, 6 bar) and 1 with the higher value (500°C, 5% wt Cu, 10 bar).*

Variable	-1	0	1
Activation Temperature, °C	300	400	500
Cu wt % in the catalyst	1	3	5
Methane pressure, bar	2	6	10

The Activation temperature (second row in table 2.1.1) refers to the calcination of copper mordenite to form and stabilize the specific active sites. According to literature, the typical experimental calcination temperatures for analogous materials are from 150°C<sup>70</sup> to 600°C<sup>58</sup>. In this case, we have worked with three calcination temperatures: 300°C, 400°C, and 500°C in an attempt to encompass a broad temperature range in which different copper site species have been reported. Copper loaded percent (% wt) (third row of table 2.1.1) is associated with the quantity of active metal sites formed in the mordenite framework and consequently with the amount of methanol produced per reaction cycle. The methane pressure (fourth row of table 2.1.1) applied in batch conditions plays a role in the reactivity of the metal sites because depending on the nature of these active sites the reactivity varies according to the methane pressure applied during the reaction. The experimental design consists of 10 experiments, in which 1% and 5% copper weight percent materials are calcinated at 300°C and 500°C separately and tested with 2 bar and 10 bar of methane pressure (they are the extreme experimental points indeed), analyzing their efficiency for the methanol obtention. While, as a central point in the experimental design, the 3% copper weight percent material, activated at 400°C, and reacted with 6 bar of methane pressure is tested by duplicate.

## **2.2. Synthesis of Materials.**

As material matrix, we employed commercial NH<sub>4</sub>-Mordenite from Alfa Aesar™ (CAS: 1318-02-1) with Si/Al mole ratio of 20 and a simplified molecular formula SiO<sub>2</sub>:AlO<sub>3</sub>. As copper precursor, we used copper (II) acetylacetonate (denoted as Cu(acac)<sub>2</sub> throughout the following pages) from Sigma Aldrich™ (CAS: 13395-16-9) with a purity of 99.9%, and whose simplified molecular formula is Cu(C<sub>5</sub>H<sub>7</sub>O<sub>2</sub>)<sub>2</sub>. We selected these materials due to their potential to incorporate and stabilize the active copper sites in the zeolite framework and donate copper ions, respectively; forming trimeric sites in 8-membered ring mordenite side pockets mainly, bringing higher yield of obtained methanol in each reaction cycle according to the results discussed in the next chapter.

The complete conversion process consists of three main steps: (i) Ionic copper exchange through calcination treatment (activation), (ii) Reaction with Methane and (iii) Washing with liquid water to pull out the methanol (see figure 2.3.2).

### 2.3. Conversion process.

#### 2.3.1.a) Ionic Copper Exchange.

For this step, we use a small ball mill during the synthesis; the employment of this tool enabled us to obtain homogeneous samples and to control the applied energy into the material during the milling. Limited by the reduced volume of this ball mill, we added 900mg of  $\text{NH}_4$ -Mordenite and 38.7 mg, 126.9 mg and 233.4 mg of  $\text{Cu}(\text{acac})_2$  to obtain the samples with 1%, 3%, and 5% copper weight, respectively (Figure 2.3.1. A), as the first step of the synthesis process. We labeled these samples as CuMor1%, CuMor3%, and CuMor5%, respectively. The milling time was of 1 hour for each sample. The added amounts of  $\text{Cu}(\text{acac})_2$  are in accordance with the maximum ion exchange allowed<sup>68</sup> by stoichiometric calculations (see Appendix 1). Which is a crucial and important point in order to obtain the specific active sites, is worth to note that similar works<sup>58,73</sup> have not taken this point into account, and did not report the methanol conversion yield. The calculus of the amount of  $\text{Cu}(\text{acac})_2$  added to the mordenite to obtain each sample (1%, 3%, and 5% wt) is shown in Appendix 2. These materials were kept in a silica desiccator in order to avoid further humidity because of the weather..

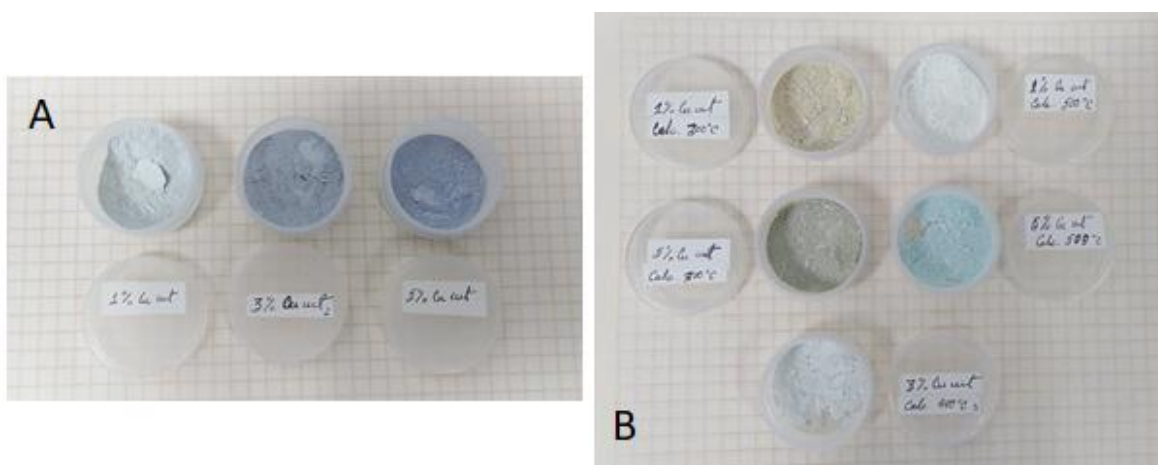


Figure 2.3.1. A.  $\text{NH}_4$ -Mordenite and  $\text{Cu}(\text{acac})_2$  after milling. B. Samples after the calcined process.

### 2.3.1.b) Calcination Treatment (Activated Materials).

In this step, we dried the samples described in 2.3.1 a) in a stove at 70°C for 24 hours and immediately kept in a silica desiccator. Later we calcined them in the presence of air in a convection muffle using a rate of 9°C/min from room temperature to 300°C and 500°C for 1% and 5% wt copper samples, and at 400°C only for 3% wt Cu sample (as a central point in the experimental design). We maintained the calcination temperature for 2 hours; and immediately after that time, cooled the system to room temperature. Figure 1, shows the as prepared samples (as described in section 2.3.1.a) previous to calcination (figure 2.3.1.A) and immediately after the heating process (Figure 2.3.1.B). After calcination at different temperatures, the activated samples are labeled as CuMorO1% 500T, CuMorO1% 300T, CuMorO5% 500T, CuMorO5% 300T, and CuMorO3% 400T. In this step of the process, we corroborate the copper loaded percent by Induced Coupled Plasma-Optical Emission Spectroscopy (ICP-OES) more detailed in Section 3 and Anexus 4, obtaining values very close to the calculated percents described in Anexus 1.

### 2.3.2. Reaction with methane.

In this step we collocated 250 mg (previously sieved through <200µm mesh) of each activated powdered material in a batch reactor system (Parr Instruments Co.) of 500 ml to carry out the reaction with methane; we did a total of 10 experiments as shown in table 3.4.1. The gaseous methane was charged into the batch reactor, containing the activated powdered material, directly from a high-pressure tank with the help of a high-low pressure manometer. Hence, the methane is in contact with the activated powdered material at room temperature. Afterwards, 2 bar and 10 bar of gaseous methane was applied to 1% and 5% samples (those previously calcinated at 300°C and 500°C, labelled as: Cu1t300p2, Cu1t300p10, Cu1t500p2, Cu1t500p10, Cu5t300p2, Cu5t300p10, Cu5t500p2, and Cu5t500p10), and 6 bar for the central point (3% wt Cu, 400°C, labelled as: Cu3t400p6a and Cu3t400p6b). We duplicate the zero-point experiment to evaluate the repeatability. We include a further experiment with conditions 1% wt Cu, calcination at 500°C and 6 bar of methane (Cu1t500p6) (see Results and Discussion 3.4 Section). The whole experiment runs in a cycle as shown in figure 2.3.2. As mentioned, the first step is the activation of the materials in the presence of oxygen from air varying the calcination temperatures. The second step is the reaction with methane at different methane pressures. Finally, the third

and last step of the process consists of the washing of the materials with liquid water to liberate the methanol chemisorbed in the copper sites.

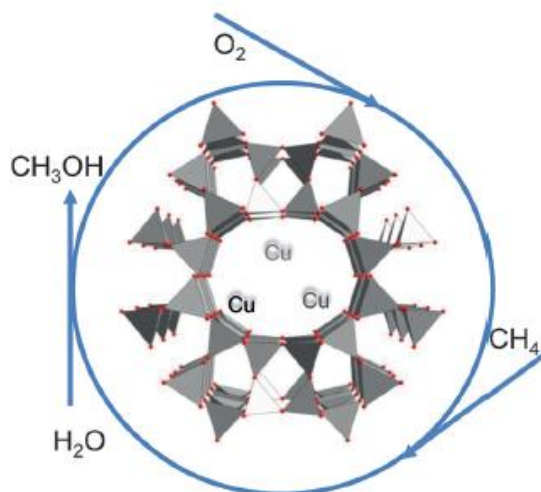


*Figure 2.3.2. Schematic representation of the whole reaction experimental cycle<sup>55</sup>. The cycle starts with the calcination step at 300°C, 400°C and 500°C in the presence of  $O_2$ , followed by the reaction with methane step (in which occurs the methane oxidation) and finally the last step is related with the methanol desorption by water washing.*

Once having the experimental conditions ready, we elevated the reactor temperature at 200°C at a rate of 2°C per minute with the use of a Parr<sup>TM</sup> heater control. The 200°C temperature was held for two hours, and subsequently, we cooled the reaction to room temperature. The applied temperature in the reaction is within the reported limit<sup>55</sup> to avoid the methane combustion and to keep the mild conditions; the low heating rate is proposed to control the reaction conditions and avoid the formation of different copper species to those already formed in the previous calcination step. At this stage of the conversion process, the material is in contact with methane at 200°C and a determined methane pressure, in order to apply the mildest conditions needed for the methane oxidation towards methanol on the active sites in the copper mordenite framework.

Concluding the previous step (reaction with methane), the reacted powdered material was recovered from the batch reactor and stored for the next step water wash with liquid

deionized water. The purpose of washing with water the reacted materials is to liberate the possible formed methanol in an appropriate liquid medium.

### **2.3.3. Sample Analysis (washing with liquid water).**

In this step, we dispersed each sample of the reacted material in 1ml of water, according to the methodology reported by Ha V. Le, *et al.*, and stirred vigorously for 30 minutes to extract the formed species in the mordenite active sites; according to the third step of the cycle. We centrifugate the liquid phase a couple of times, then filtrated (2 $\mu$ m filter) in each wash and preserved in vials at 4°C until the chromatographic analysis. In order to quantify the resulting product, before chromatographic analysis, we added 1 $\mu$ L of Isopropyl Alcohol (IOH) to each sample as an internal standard. We carried out Gas Chromatography-Mass Spectrometry (GC-MS) analysis in a Clarus SQ 680 Gas Chromatograph coupled to a Clarus SQ 8T Mass Spectrometer (Perkin Elmer, Boston, MA, USA), using a PE-WAX (Pekin Elmer) capillary column (50m x 0.25mm x 0.25 $\mu$ m phase thickness). Setting the temperature program as follows: 40 °C for 8 min, 20 °C/min up to 80 °C, 40 °C/min up to 90 °C and 50 °C/min up to 180 °C. The injection temperature was 150 °C, and helium was used as carrier gas (1.5 mL min<sup>-1</sup>). The mass spectrometer was operated in electronic impact mode (70 eV), with selective ion monitoring (m/z 29, 1, 43, 45, 46, 58, 59 and 60, dwell time 0.05 s), keeping the chromatograph interphase and the source temperature at 280 °C. We performed the methanol quantitation (mz 29+31) and IOH (m/z 45) using a five-point calibration curve (R > 0.99, shown in Appendix 3) and areas of specific ions mass-chromatograms.

### **2.4 First observations derived from the synthesis pathway.**

NH<sub>4</sub>-Mordenite does not present any change before and after the calcination process in the temperature range chosen to. To produce some structural changes in zeolites, it is required to apply much more energy than what we are currently working<sup>61,90</sup>; for this reason, our synthesized materials do not present any relevant structural changes in any step of the described conversion process, as it is shown in X-Ray Diffraction Section and Infrared Spectroscopy. In the case of copper exchanged samples, some color changes occurred as a function of the loaded copper amount and the activation temperature. The samples calcined at 300°C presented a dark-grey blue color, while the ones calcined at

400°C produce very light blue tones, similar appearance is found in samples activated at 500°C, with slight light blue variations (see figure 2.1 experimental section). The color differences between the samples calcined at 300°C, 400°C and 500°C come from the residues of Cu(acac)<sub>2</sub> carbonization; it is known that the dark tones in the 300°C activated samples come from the presence of carbonized matter<sup>68</sup>. The light blue color of samples calcined at 400°C and 500°C can be attributed to the formation of CuO particles in mordenite<sup>91</sup>.

The calcined samples differ from pure H<sub>4</sub>-Mordenite, the previous ones have a fine powder aspect while the NH<sub>4</sub>-mordenite presents a consistency of big lumps, probably due to the water absorbed in long time storage. NH<sub>4</sub>-Mordenite have a high electrostatic interaction with materials that tend to disappear once the copper is present in mordenite structure as a cation, stabilizing its natural negative framework.

### 3. RESULTS AND DISCUSSION.

In the following chapter, we present the main results of the work supported by a discussion based on the information previously presented in chapter 1 (Theoretical Framework) and chapter 2 (Experimental Section). At first, we discuss some observations of the materials in the synthesis pathway and reaction. After, we describe each analysis done with a brief explanation of the measurement conditions. To quantify the quantity of obtained methanol in each experiment, we employed the Gas Chromatography-Mass Spectrometry (GC-MS) technique. With the collected data from the GC-MS, we propose a statistical model which describes the complete experiment in the range of the variables studied. In order to follow the changes in the materials and the appearance of new copper species, which are responsible of the methane to methanol conversion, we applied a combination of different spectroscopical techniques: Electronic Spectroscopy, Infrared Spectroscopy, and Electron Paramagnetic Resonance. We employed Induced Coupled Plasma-Optical Emission Spectroscopy, Thermogravimetric Analysis, Scanning Electron Microscopy-Energy Dispersive X-Ray Spectroscopy and Adsorption Isotherms (BET Analysis) to provide further information about the changes produced by copper exchange and calcination in each step of the conversion process.

#### 3.1 Catalyst Characterization.

- Scanning Electron Microscopy and Electron Dispersive X-Ray Spectroscopy (SEM-EDS).  
Micrographs and EDS measurements were acquired with a JEOL scanning electron microscope, model JSM-6390. In the 10  $\mu\text{m}$  - 2.5  $\mu\text{m}$  range, at 20 kV voltage and vacuum. By EDS were analyzed oxygen, aluminum, silicon and copper obtaining the weight percent and the atomic percent.
- N<sub>2</sub> Sorption Analysis.  
The N<sub>2</sub> Adsorption Isotherms were recorded at 75K in the pressure range of 10<sup>-1</sup>-250 Torr using an ASAP 2020 analyzer from Micromeritics. Before analysis, the samples were degassed at 170°C for 12 hours. The surface area was determined by BET analysis.
- Powder X-Ray Diffraction (XRD).

Wide angle XRD powder patterns were recorded with  $\text{CuK}\alpha_1$  ( $\lambda=1.54056 \text{ \AA}$ ) radiation in a D8 Advance diffractometer from Bruker, equipped with a Lynx Eye Detector.

- Gas Chromatography-Mass Spectrometry (GC-MS).

GC-MS Analysis of the resulting products and seeking for desired products as methanol was done in a Clarus SQ 680 Gas Chromatograph coupled to a Clarus SQ 8T Mass Spectrometer (Perkin Elmer, Boston, MA, USA), using a PE-WAX (Pekin Elmer) capillary column (50m x 0.25mm x 0.25 $\mu\text{m}$  phase thickness). For a complete description of the conditions employed in the GC-MS measurement see 2.3.3 section.

- Induced Coupled Plasma-Optical Emission Spectroscopy (ICP-OES).

ICP-OES technique was employed to corroborate the copper weight percent in synthesized materials. It was employed a Perkin Elmer ICP-OES Optima 8000 Model. For data treatment it was employed Winlab software. For copper quantification it was employed a calibration curve in the range of 0-70 mg/L and an emission line of 327.393 nm.

- Digestor.

Titan MPS Perkin Elmer microwave sample preparation system was employed to digest the copper exchanged zeolites. We use 100 mg of the copper mordenite samples mixed with 1.0 mL of  $\text{HNO}_3$ , 3.0 mL of  $\text{HCl}$ , and 1.0 mL of  $\text{HF}$  as acid reagents with the following temperature program, see table 3.1.1.

Table 3.1.1. Temperature program for materials digestion.

Step	Target Temp [°C]	Pressure max [bar]	Ramp Time [min]	Hold Time [min]	Power [%]
1	170	30	2	50	80
2	190	30	2	5	90
3	230	35	2	10	100
4	50	35	1	10	0
5	-	-	-	-	-

- UV-Visible Spectroscopy (UV-Vis).

UV-Vis spectra were collected in diffuse reflectance mode with a Perkin Elmer spectrometer equipped with an integrating sphere. Alumina was employed as a white standard. Spectra were taken from 200 to 800 nm with a step size of one nanometer. Results are presented in the Kubelka-Munk function (see Appendix 7) obtained from acquired reflectance data.

- Fourier Transform Infrared Spectroscopy (FTIR).

FTIR spectra were run using KBr pressed pellets with a Spectrum One Spectrophotometer from Perkin Elmer. Spectra were taken from 4000 to 250  $\text{cm}^{-1}$  with a 2  $\text{cm}^{-1}$  step. To compare the samples with each other, we employed 20mg of KBr per 2mg of the studied material in the different stages of the conversion process.

- Thermogravimetric Analysis (TG).

The TG curves were recorded under a nitrogen flow of 100mL/min in a modulated high-resolution thermobalance (Q500 from TA Instruments), using a high-resolution dynamic method with a heating rate of 3°C  $\text{min}^{-1}$ . The data was acquired in a temperature range from room temperature to 900°C.

- Electron Paramagnetic Resonance (EPR).

(falta)

### 3.2 X-Ray Diffraction Analysis

In order to verify if the copper exchange had made structural changes throughout the reaction cycle or the formation of copper species anchored to the mordenite framework we employed the X-ray Diffraction (XRD) technique. XRD patterns were done to the pure  $\text{NH}_4$ -Mordenite, the exchanged samples (just milled) and the calcinated samples with the purpose to evaluate the possible structural changes that may occur in the materials after copper insertion and calcination (see figure 3.2.1).

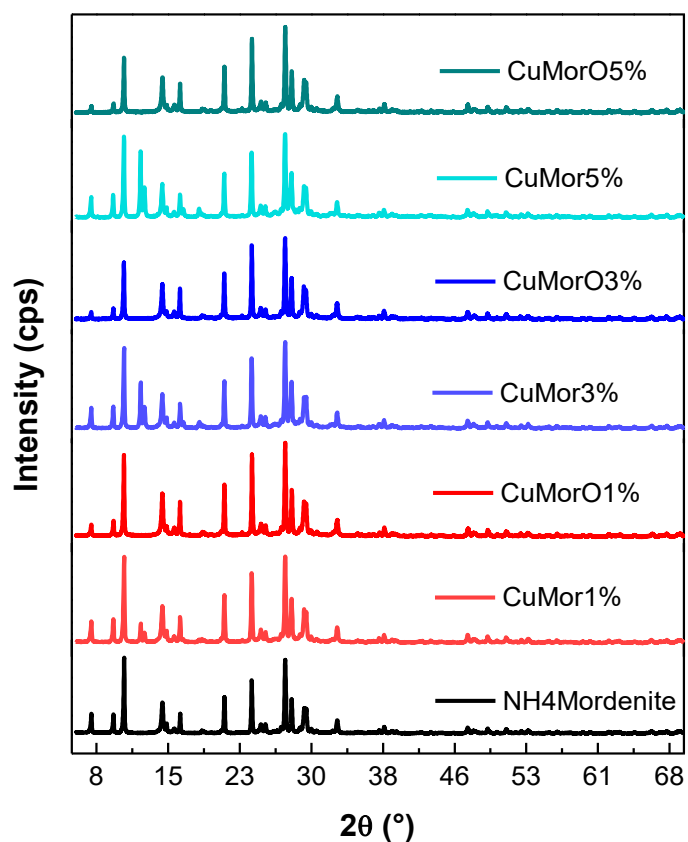


Figure 3.2.1. X-Ray diffraction patterns for clear pure  $\text{NH}_4$ -mordenite (black), the milled exchanged samples (CuMorO 1%, 3% and 5%) and the calcinated ones samples (CuMor 1%, 3% and 5%).

XRD measurements shown in figure 3.2.1, demonstrate that the structure of calcined copper mordenites is in agreement with the parent mordenite ( $\text{NH}_4$ -Mordenite). No additional peaks specific for elemental copper or its oxides were detected in the calcined samples patterns suggesting that the copper species are highly dispersed throughout the

mordenite framework, and that copper-based nanoparticles, if any, are smaller than three nanometers<sup>68</sup>. It seems that the smaller effective ionic radius for copper (II) ion in solid-state exchange favors its intra-crystalline diffusion and the access to the possible positions for the charge balancing cation<sup>58</sup>. The exchanged samples pattern showed a clear difference with respect to the calcined ones: they presented a mixture of two phases concerning with NH<sub>4</sub>-Mordenite and Cu(acac)<sub>2</sub>. The combination of these two phases occurs because the only present phenomena in the milling process is the diffusion of Cu<sup>2+</sup> ions through the mordenite framework, but the acetylacetonate do not react or make chemical bonds with NH<sub>4</sub>-mordenite. The XRD patterns of calcinated samples present one phase associated with NH<sub>4</sub>-Mordenite (figure 3.2.2), without the appearance of any relevant change in the pattern that suggests the formation of a specific copper species due to we could not observe the formation of any new peaks, nor a shift or a notorious change in peak intensity that would suggest the formation of some copper species. (the identified phase is the PDF 00-043-0171|Sodium Ammonium Silicate Hydrate which corresponds with the NH<sub>4</sub>-Mordenite Employed). This is an expected behavior given that the disappearance of all traces of Cu(acac)<sub>2</sub> by heating is favored<sup>68</sup>. Avoid These carbon traces species presence from acetylacetonate is desirable, otherwise they could hinder the methanol yield<sup>7</sup>during the conversion process. The phases identification was done with EVA Software (Bruker<sup>TM</sup>) employing the PDF4 crystallographic database.

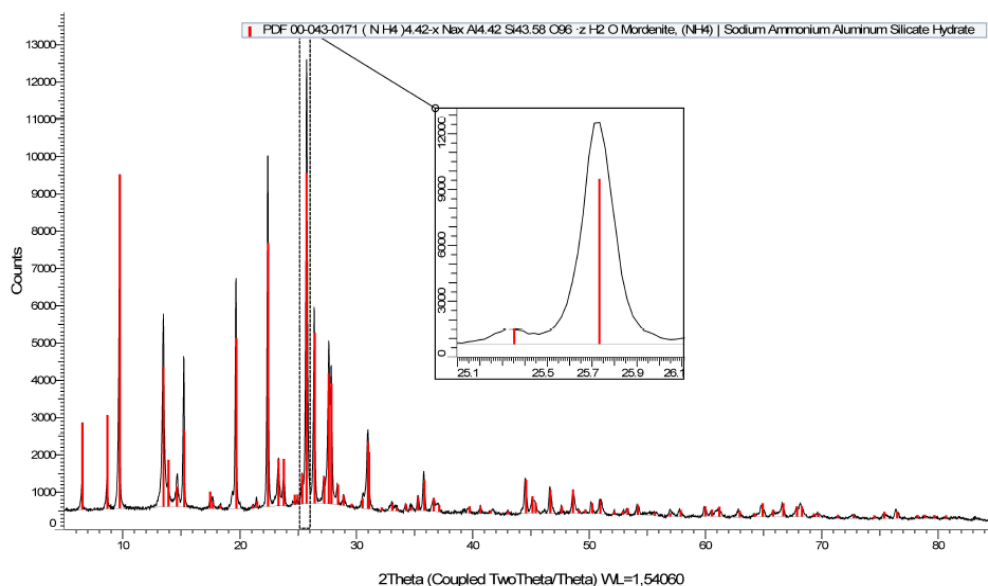


Figure 3.2.2. Phase identification of CuMorO3% 400 T.

In figure 3.2.2 we present a phase identification of CuMorO3% 400T sample, we found that the phase corresponds to the NH4-Mordenite. In the inset we can observe the correspondence with the main peak with a good centrality. Suggesting a correcting phase identification process.

### 3.3 Scanning Electron Microscopy-Energy Dispersive X-Ray Spectroscopy.

We resort to Scanning Electron Microscopy (SEM) technique to analyze the morphology of the calcinated samples at 500°C (CuMorO1% 500T and CuMorO5% 500T) and 400°C (CuMorO3% 400T), presented in figure 3.3.2. In order to evaluate if the higher calcination temperature (in the worked range) produced morphological changes. The micrographs are shown in figure 3.3.2. (first and second row) , present big cumulus in the micrometers range size. These cumuli are not uniform in shape but in size. The calcined materials (figure 3.3.2, first and second row) seems to occur in clusters of closely spaced cumulus in the form of fibrous aggregates, and the filaments commonly intertwine into packed mesh-like structures<sup>27</sup>. This shape features observed in SEM range scale could be hinder the methanol conversion due to the low contact between the methane and the active copper sites at room pressure as reported by Priya, *et al.*<sup>27</sup>, requiring probably higher pressures and temperatures so as to increment their contact inside the cumulus, however, by GC-MS we have found that pressure does not seem to have a relevant role in methane conversion to methanol in a batch reactor, so that a detailed TEM measurements are needed in order to shed light about this as reported by Park, *et al.* The pure mordenite sample showed needle-like crystalline morphology, a typical characteristic of mordenite zeolites<sup>92</sup> (figure 3.3.1). Also, the micrograph of calcined copper samples was compared

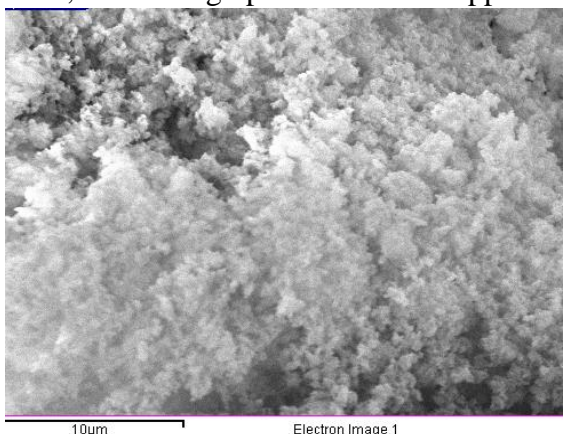
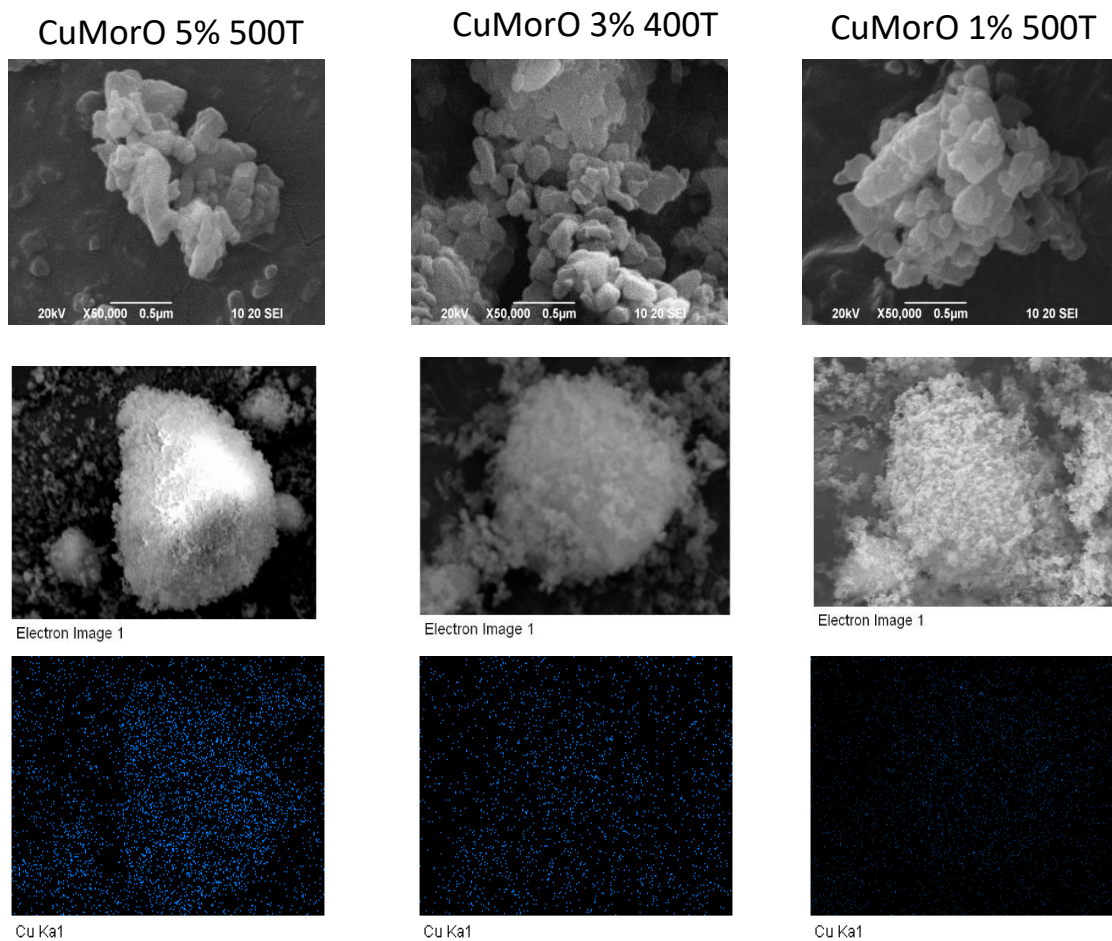


Figure 3.3.1. SEM micrography of NH4-Mordenite.

with the pure Mordenite<sup>93</sup>, observing approximately the same cumulus shape and size (not shown), so the copper insertion does not modify the morphology entirely at this scale. Unfortunately, it was not possible to make a micrograph of isolated copper clusters due to the detection limit of this technique and the low probability to locate a specific copper cluster (less than 3nm) in the physical area of the image.

Energy Dispersive X-Ray Spectroscopy (EDS) measurements were done in the same region of the samples analyzed by SEM. The analyzed elements were Copper, Silicon, Aluminum, and Oxygen. The third row of figure 3.3.2 shows in blue color the copper identification per area; we observe an increased intensity of copper dots according to the



*Figure 3.3.2. SEM micrographs and EDS copper analysis of CuMorO5% 500T (left column), CuMorO3% 400 T (middle column), and CuMorO1% 500 T (right column) samples.*

amount of copper inserted. That can be caused due to the size of the copper clusters formed during the activation process; according to previously reported results<sup>7,55,56</sup>. Furthermore, we observe a similar distribution of copper dots in the area of the three samples. However,

it is not possible to ensure that the observed dots correspond to active copper sites due to the equipment mounting base is made of copper, this fact brings uncertainty about the accuracy of the measurement. According to the EDS measurements, the atomic copper percent for CuMorO1% 500T is of 1.2%, for CuMorO3% 400T is 2.4%, and CuMorO5% 500T is 4.09%, nearly to the copper weight percent. The apparent good distribution of the copper points in the material is not conclusive to affirm that we have a homogeneous sample, but, it gives us an idea about a good enough dispersion of copper in the mordenite framework. The population and distribution of silicon, aluminum, and oxygen are approximately constant for all samples analyzed by EDS. Also, they are higher and definer than copper because they are an inherent part of the mordenite structure and the atomic percent of all of them represent almost the whole percentage from the analyzed materials (from ~95-98.8%).

#### **3.4. Gas Chromatography-Mass Spectrometry Analysis.**

As mentioned in the last step of the conversion method (see section 2.3.3), washing with liquid water to pull out the methanol), the wash water (filtrated) of each sample was analyzed with GC-MS. Information of experimental conditions and quantity of methanol obtained is presented in table 3.4.1. The best result was obtained by the Cu3t400p6b test, with a total of 29.840  $\mu\text{mol/g}$  and 0.0632  $\mu\text{mol Met}/\mu\text{mol Cu}$ . This sample, corresponding to the second test of the central point in the experimental design, contains 3 wt% copper, was activated at 400°C and reacted with 6 bar of methane. No methanol was detected after the interaction of methane with the activated  $\text{NH}_4$ -Mordenite; this proves that the presence of copper species is essential for the conversion of methanol from methane. On the other hand, the samples with higher and lower quantity of copper-loaded (5 wt% and 1 wt%, respectively), on the contrary, showed a decrease in the amount of methanol obtained. Using a global analysis per variable (obtained with an ANOVA, acronym of Analysis of Variance) that consists of a statistical analysis that let to see the contribution to the methanol yield per variable. This study was extended to investigate the influence of the amount of copper-loaded in mordenite via solid-state ion exchange on the methanol production. In figure 3.4.1, it is shown the behavior of the methanol results presented in table 3.4.1, as a function of the quantity of copper inserted.

Table 3.4.1. Summary of experimental conditions and amounts of methanol obtained in  $\mu\text{mol/g}$  and  $\mu\text{mol/mol Cu}$  units. The variables -1, 0, and 1 correspond to the established values described in table 2.1.1 According to nomenclature, the name of each test suggests the synthesis via and the reaction conditions employed.

Samples	Cu wt %	Activation Temperature	Pressure	$\mu\text{mol/g}$	$\mu\text{mol Met/mol Cu}$
cu1t300p10	-1	-1	1	11.215	0.0713
cu1t300p2	-1	-1	-1	4.732	0.0301
cu1t500p10	-1	1	1	20.732	0.1317
cu1t500p2	-1	1	-1	17.289	0.1099
cu5t300p10	1	-1	1	15.636	0.0199
cu5t300p2	1	-1	-1	3.098	0.0039
cu5t500p10	1	1	1	21.206	0.0270
cu5t500p2	1	1	-1	8.460	0.0108
cu3t400p6a	0	0	0	24.745	0.0524
cu3t400p6b	0	0	0	29.840	0.0632
cu1t500p6	-1	1	0	6.596	0.0419

Milder and lower performances were obtained here in comparison with those reported in the literature<sup>55,56,68,94</sup>. These performances are a consequence of the employed experimental conditions, the volume of the batch reactor according to the amount of material reacted probably diffculted the interaction between the sample active sites and the methane available for the reaction, furthermore, the manipulation of the material in each step of the conversion process incremented the uncertainty of the results. Better experimental conditions are needed in order to increase the Methanol conversion yields (e.g., continuous flow reactor).

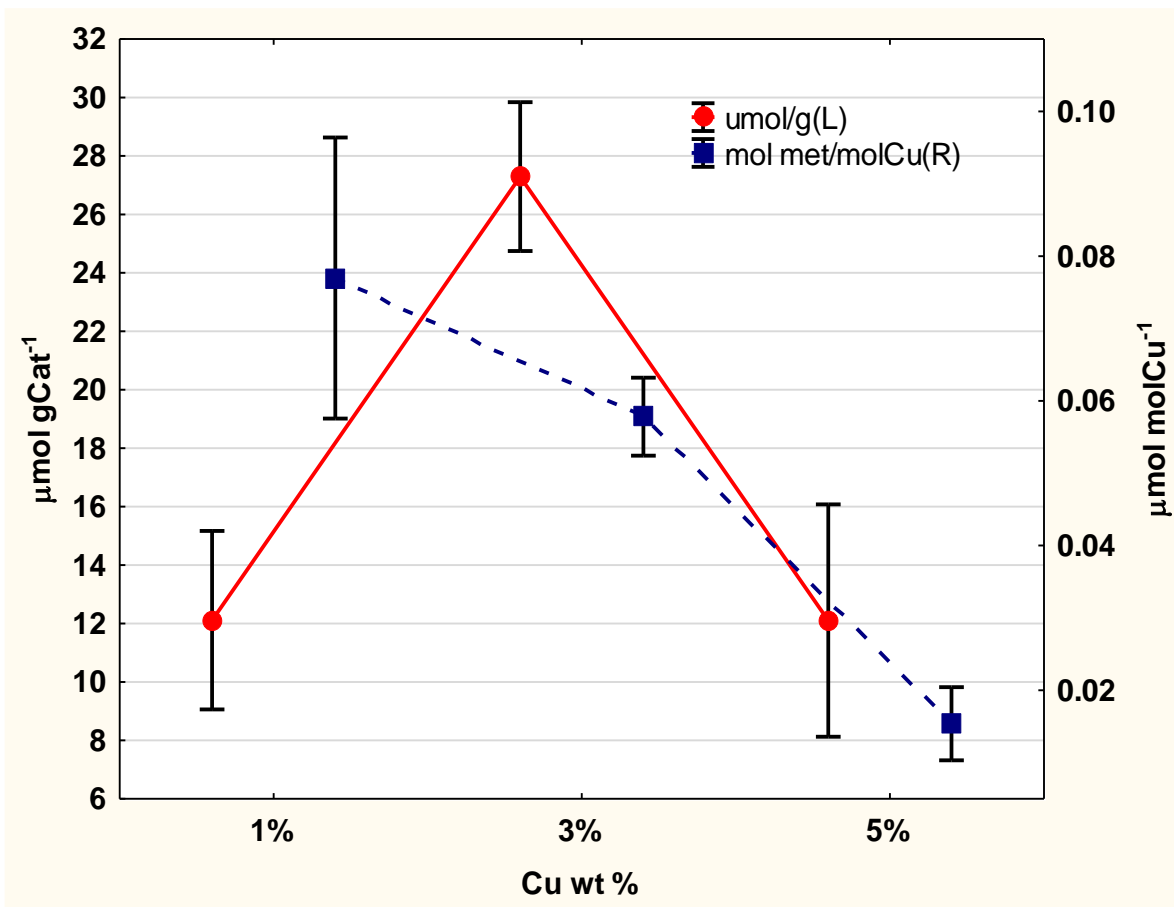


Figure 3.4.1. Methanol obtained versus copper weight percent.

According to a global analysis per variable, at low and high copper loadings (1 wt% and 5 wt%, respectively) were obtained low methanol conversion quantities, 12  $\mu\text{mol/g}$ , with a significant uncertainty for 5 wt% samples. As expected, the TON behavior increased approximately from 0.02 to 0.08 by reducing the copper loading from 5 wt% to 3 wt%; this is according with the reported in the literature<sup>68</sup>. By stoichiometric calculation, the maximum amount of copper that can be exchanged in mordenite is between 4% and 5% copper weight percent (Appendix 3); this suggests that for the samples with 5 wt%, not all the copper loaded is producing active sites. Part of the copper can be forming another species or being part of a phenomenon that might produce a negative effect in methanol yield, as occurs with sintered copper; or it is possible that not all species were formed, at the temperatures and pressures ranges worked in this contribution. In the case, for 1 wt% and 3 wt% copper samples, it is observed an increasing tendency in methanol yield, probably owing to the relation between the quantity of copper-loaded and an increase in the formation of sites reactive to methane without exceeding the maximum number of

potentially available sites in the framework structure according to stoichiometric calculations. At the end, in this kind of materials, lower quantities of exchanged copper-loaded tend to produce more methanol than those reported with 50 wt% Cu<sup>58,68</sup>.

In the case of temperature and methane pressure global analysis per variable, presented in figure 3.4.2, the results are as expected. The temperature has an increasing linear behavior in the studied range, explained by the fact that at higher temperatures the contact between methane and the copper mordenite increase due to an increase in kinetic energy of

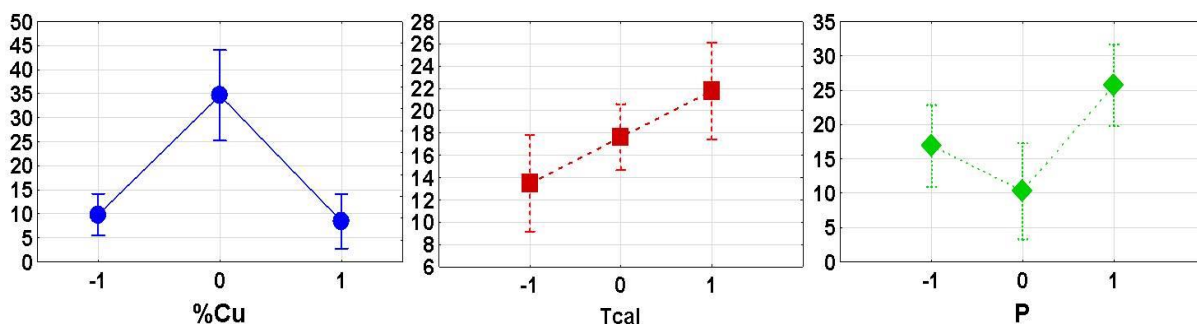


Figure 3.4.2. Methanol obtained versus copper loaded (%Cu, left), activation temperature (Tcal, middle) and methane pressure (P, right). Variables values -1, 0, 1 are presented in Table 1 of the experimental section.

molecules, reaching more methane molecules to the active copper sites in a specific time. The pressure presents a decrease in the reaction at 6 bar and an increasing tendency between the 2 bar and 10 bar; this suggests that this variable does not play a relevant role in this experiment in the methanol yield since the best results were obtained by the same central points.

The complex dependency of  $\mu\text{mol/g}$  yield as a function of two variables (calcination temperature (Tcal), pressure (P), and copper weight percent (%Cu)) is shown in figure 3.4.3, in which the minimal partial square adjusted surface graphics can be appreciated. It is noticeable that quadratic relations are needed given the shape adopted by the curve shown in the figure 3.4.3. Indeed, the analysis of complete factorial experimental design  $2^k$  with a pair of central points does not show a relevant influence of any variable and a suitable adjust neither if it is not taking into account the curvature (Curv) parameter in the analysis design. After eliminating the non-significative effects, it is obtained a model with an intercept in which only the variables Tcal, P and Curv are significative.

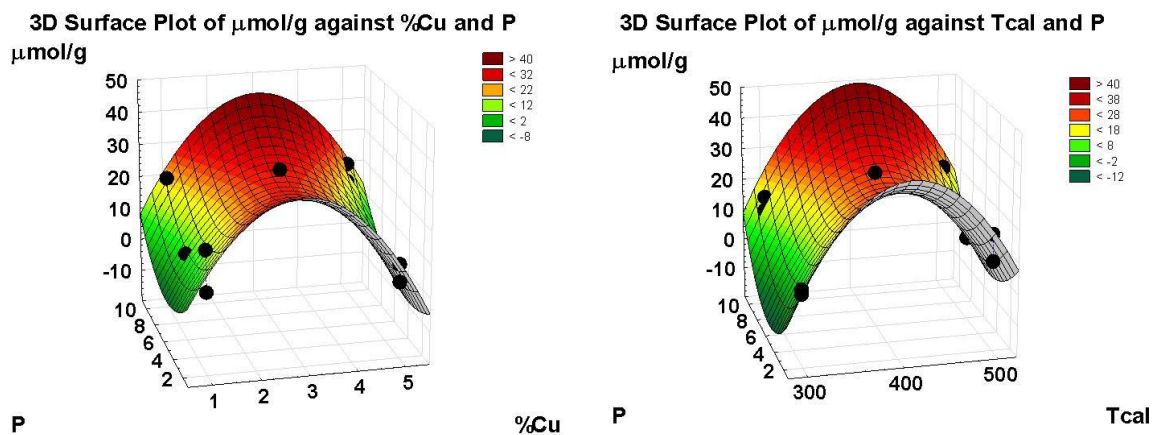


Figure 3.4.3. Yield conversion dependence with respect %Cu, Tcal and P.

The values predicted by the model, compared with the values obtained from the experiment, are shown in table 3.4.2. It must be noted that comparing the data obtained and predicted, the model does not offer sufficient certainty. At this point, the main effects analysis obtained by the ANOVA showed the global influence of variables in methanol production in the studied range. The different behavior of each single variable is clearly appreciated in figure 3.4.2. according to the experimental design.

Table 3.4.2. Observed versus predicted values with the first model with the curvature and intercept.

Samples	Observed ( $\mu\text{mol/g}$ )	Predicted ( $\mu\text{mol/g}$ )	Residuals
cu1t300p10	11.21507	13.07158	-1.85652
cu1t300p2	4.73229	4.26898	0.46332
cu1t500p10	20.73241	21.32311	-0.59071
cu1t500p2	17.28864	12.52050	4.76814
cu5t300p10	15.63592	13.07158	2.56433
cu5t300p2	3.09784	4.26898	-1.17113
cu5t500p10	21.20600	21.32311	-0.11711
cu5t500p2	8.46018	12.52050	-4.06032
cu3t400p6a	24.74549	27.29259	-2.54709
cu3t400p6b	29.83968	27.29259	2.54709

As mentioned above, the experimental model with curvature does not offer an extremely accurate explanation of the influence of the variables in methanol yield. Therefore, it was employed a polynomial regression (Table 1, Appendix 5), in which it is observed an influence of cooper weight percent %Cu and pressure P with a good description of the results. Figure 3.4.4 shows how far away the experimental data are from those predicted by the proposed model, and although the approximation is good, it can be improved by making a nonlinear consideration.

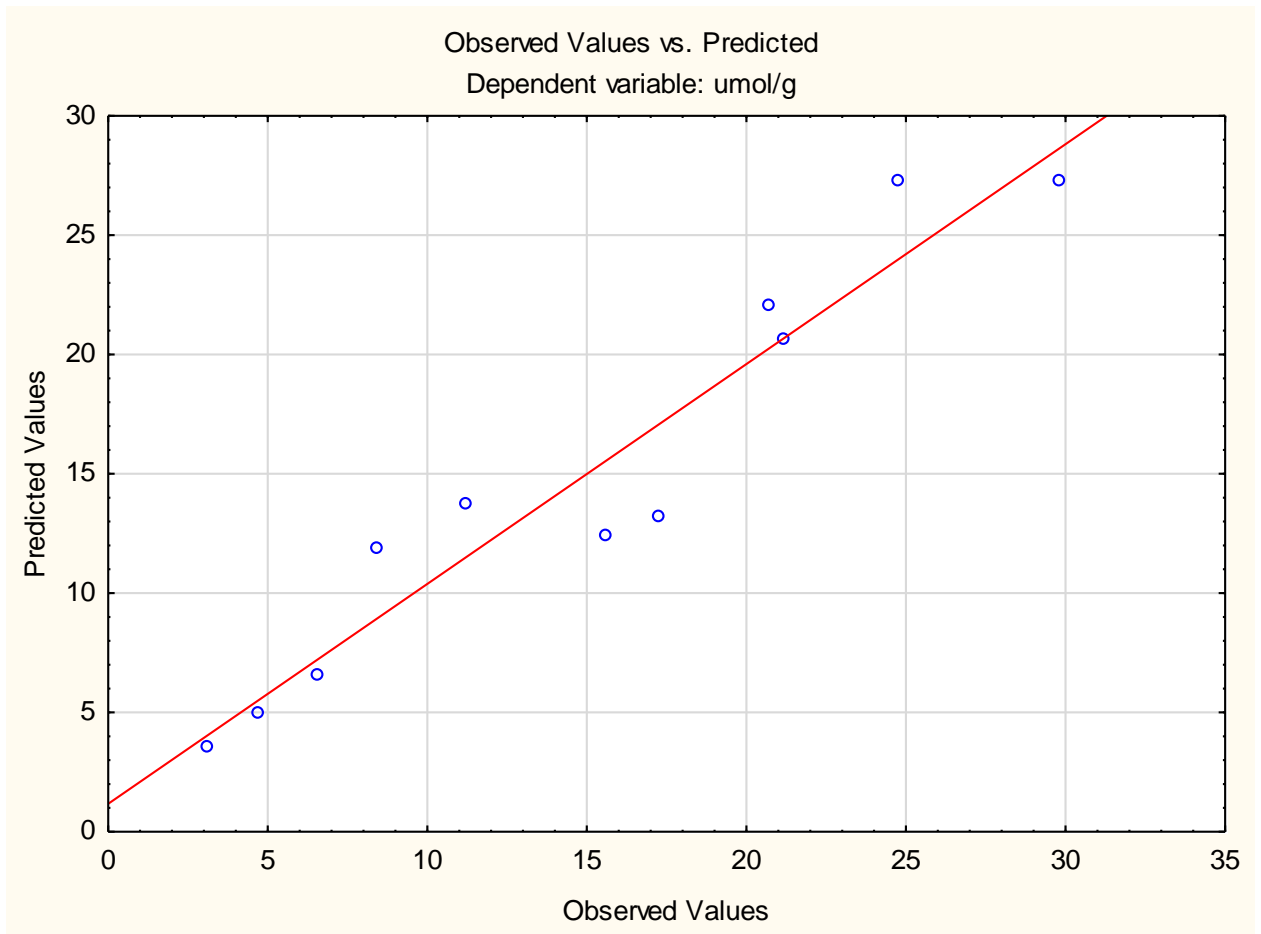


Figure 3.4.4. Predicted vs Obtained results by the polynomial regression model.

Finally, in order to obtain a model based on the real values of the variables, it was proposed a nonlinear function estimation. The predicted results can be compared with the experimental ones (Table 2 of Anexus 5). Using this nonlinear function estimation, the residuals are lower than the previously discussed models, suggesting a better approximation comparing with the polynomial regression. The next equation describes

the obtained model, note that %Cu and P variables acquire a quadratic form as we can infer from figure 3.4.3, while Tcal is the only variable with linear dependence with the yield. A, B, C, L, Q, and R represent the coefficients that, according to the conversion analysis, show the better fit of the experimental data.

$$Yield = A + B * \%Cu + C * (\%Cu)^2 + L * Tcal + Q * P + R * P^2 \quad \text{equation (3.1)}$$

All terms were considered because, as can be seen in table 3.4.3, the least significant effect is very close to a p-value of 0.5. In the same table we can observe the estimate values of coefficients presented in equation 3.1 according-to the nonlinear model.

*Table 3.4.3. Estimated values of coefficients according to nonlinear model, the t-value corresponds to the coefficient divided by its standard error; the standard error is an estimate of the standard deviation of the coefficient, it can be thought of as a measure of the precision with the regression coefficient is measured. P value is referred to a significance level of the coefficient (<0.05).*

Model Coefficients	Estimate Coefficients Values	Standard error	t-value	p-value
A	-27.38556178	6.924668	-3.95478	0.010799
B	37.92969080	6.752472	5.61716	0.002475
C	-6.37961990	1.148429	-5.55508	0.002599
L	0.04125764	0.012277	3.36050	0.020097
Q	-7.16612603	3.069305	-2.33477	0.066813
R	0.68887102	0.254493	2.70683	0.042436

This nonlinear model fits better the experimental points obtained for methanol conversion. The comparison table of observed versus predicted results can be found in table 2, Appendix 5. The residues normality graph and residues against the predicted values shows the correctness of the analysis performed (figure 1 and 2, Appendix 5).

### **3.5 Induced Coupled Plasma-Optical Emission Spectroscopy Analysis.**

From the information obtained with Induced Coupled Plasma-Optical Emission Spectroscopy (ICP-OES), we evaluate the copper quantity in the synthesized materials after the heating treatment: CuMorO1% 500T, CuMorO5% 500T, CuMor3% 400T.

To analyze the samples, we digest 100 mg of each of them with a mixture of Nitric acid, Hydrochloric acid, and Fluoride acid (1ml, 3ml, 1ml, respectively) with a Perkin Elmer

Microwave system with a stepped power process, with a maximum temperature of 250°C (Data obtained in appendix 4).

As shown in table 3.5.1, the copper loaded per cents of 1%, 3%, and 5% correspond with the calculated ones (see section 2.3.1.a and Appendix 2). Also, it seems that the heat treatment does not change the copper quantities because the values obtained of copper weight percent are very proximal to calculated, suggesting that this step of the process does not produce relevant changes in copper amounts.

*Table 3.5.1. ICP-OES copper results for calcinated samples.*

Sample	Measured Concentration (mg/mL)	Copper mass (mg)	wt% Cu
CuMorO1% 500T d10	0.011	1.1	1.1%
CuMor3% 400T d10	0.031	3.1	3.1%
CuMorO5% 500T d10	0.05	5	5%
CuMorO1% 500T	0.093	0.93	0.93%
CuMor3% 400T	0.289	2.89	2.89%
CuMorO5% 500T	0.481	4.81	4.81%

### 3.6 Thermogravimetric Analysis.

By thermogravimetric analysis (TGA), we found changes in the total weight percent concerning the liberation of material's components through the heating process. In both figures, 3.6.1 and 3.6.2, we observe three main weight losses For NH<sub>4</sub>-Mordenite and Cu3%, respectively. For NH<sub>4</sub>-Mordenite (figure 3.6.1) near 100°C, a considerable weight loss of 10% is observable (Appendix 6) associated with physically sorbed water located in the cavities of materials<sup>58</sup>. The fall between 200°C to 400°C (nearly 2% weight loss) is attributable to interacting water with the material framework, or possibly due to gradual liberation of chemisorbed water. A visible loss near 500°C is related to ammonia liberation, which begins before all the physi-sorbed water is removed<sup>90</sup>. The ammonium atom, during the calcination process, tends to decompose to ammonia and residual hydrogen ions. The decay occurs approximately from 500°C up in ammonium mordenite.

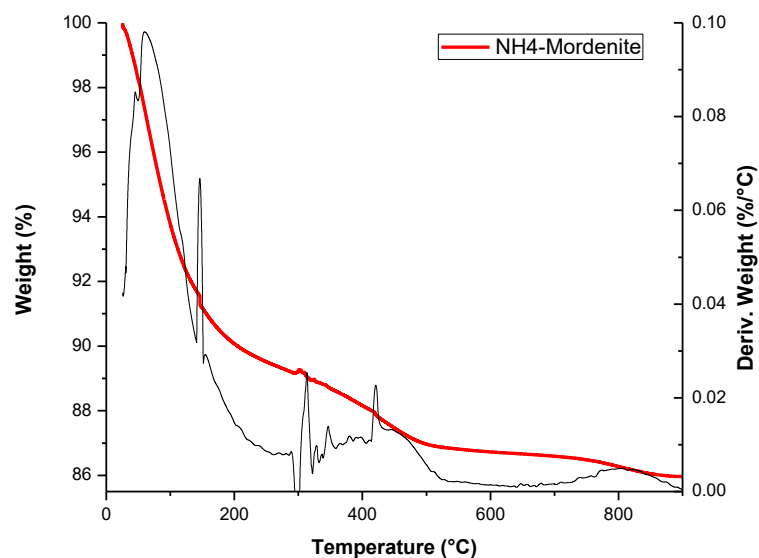


Figure 3.6.1 Thermogravimetric decomposition of NH4-Mordenite.

At this stage of decomposition, the hydrogen ions tend to form Brönsted Acid species with mordenite framework with the formula  $\text{HAlSi}_7\text{O}_{16}^{90}$ . The final step in the thermal decomposition of NH<sub>4</sub>-Mordenite is the removal of hydrogen ion as water (at 800°C) from the mentioned Brönsted Acid species<sup>90</sup>. The total weight loss in the studied temperature range corresponds to 14% (Appendix 6, Figure A).

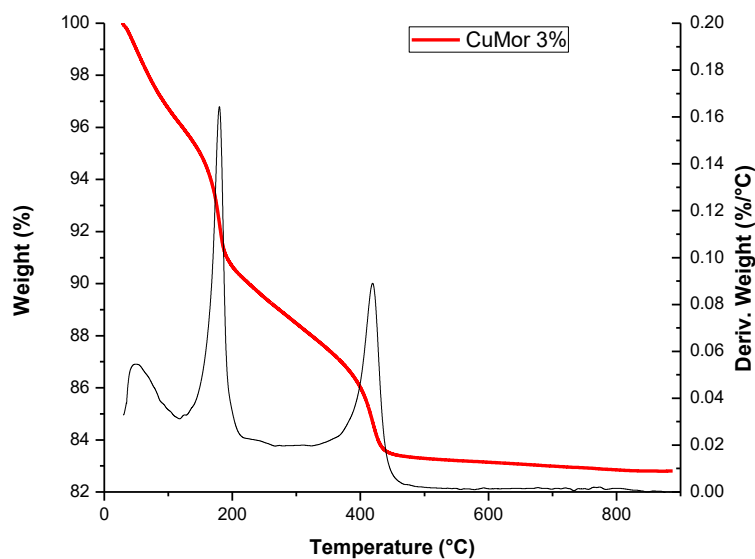


Figure 3.6.2. Thermogravimetric decomposition of CuMor 3% sample.

For CuMor3% sample, we observe three well-defined weight losses (See black derivative curve in figure 3.6.2). The first loss, between 30°C and 100°C, correspond to water located in the mordenite framework<sup>58</sup> (3.6% weight loss). The second one, starting at 170°C is related to the boiling point of acetylacetonate leaving the mordenite framework, remaining the copper (II) ions from the Cu(acac)<sub>2</sub> molecules. Also, near this temperature occurs the detachment of chemisorbed water and weakly attached OH groups and H terminals<sup>90</sup> (5.6% weight loss). Acetylacetonate release remains as temperature increases; it is present with the release of physisorbed water in the range between 200°C-400°C. The final weight loss near 400°C is related with the ammonium decomposition<sup>90</sup> and the ammonia liberation. Any other loss at higher temperatures is not appreciable, suggesting a previous ion exchange in the milling process with consequences in the ease of release of hydrogen ions<sup>58</sup>.

### **3.7 Adsorption Isotherms (BET Method).**

Only the calcined samples and pure mordenite were analyzed by adsorption techniques (CuMorO5% T500, CuMorO5% T500, CuMorO3% T400, CuMorO1% T300, CuMorO1% T300 and NH<sub>4</sub>-Mordenite). Based on the TGA results, we chose the degassed temperature applied for the adsorption analysis, 200 °C for 12 hours, corresponding to the dehydration temperature, closely coinciding with the reported conditions used for analogous materials by Samira Parishan, et al<sup>68</sup>. Knowing that mordenite has a set of sizeable porous structure compared with other zeolites employed for methane to methanol conversion (previously discussed in the theoretical framework section), we used nitrogen (N<sub>2</sub>, whose kinetic diameter<sup>86</sup> is of 3.6 Å) as a probe molecule to perform the adsorption studies avoiding any kind of steric restriction. The active copper sites, formed during calcination, are reported to be located in the 8-Membered ring side pockets mouth pore<sup>12,95</sup> which are part of the straight channels surface large aperture composed of 12-membered rings, through them the N<sub>2</sub> can be transported. This suggests that the size of the pore windows is large enough to allow the diffusion of the N<sub>2</sub> molecules through the porous framework.

$N_2$  is a stable molecule with a quadrupole moment. This feature let it function as a sensor for the local electric field gradient inside the absorbent cavities<sup>96</sup>. Consequently, adsorption isotherms offer information about the electronic structure of our materials. For all samples (NH<sub>4</sub>-Mordenite, CuMor1% 500T, CuMor5% 500T, CuMor1% 300T, CuMor5% 300T, and CuMor3% 400T), it is observed a not pronounced hysteresis loop for long equilibrium times, especially for NH<sub>4</sub>-Mordenite and CuMorO3%, see appendix 8. This behavior suggests a low strength guest-host interaction allowing a good molecule diffusion through the porous framework as discussed in the DRX section. It seems that the molecule absorption close to active copper sites is favorable for the transport of other molecules through the NH<sub>4</sub>-mordenite channels. Furthermore, we observe that the  $N_2$

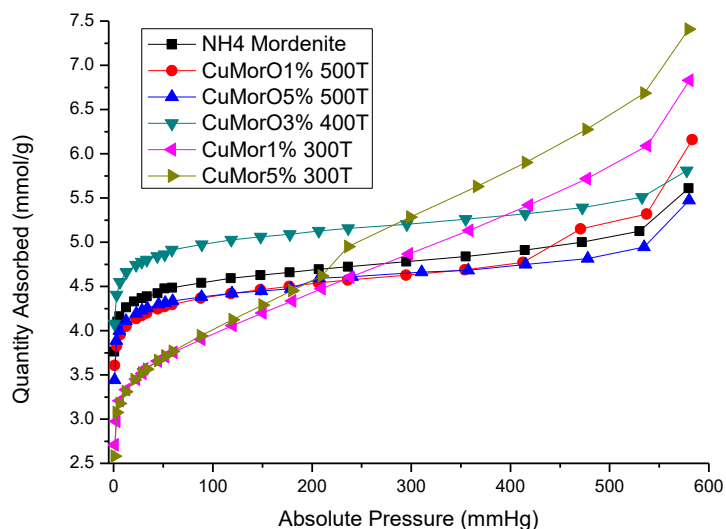


Figure 3.7.1. Adsorption isotherms of activated materials, degassed at 200°C for 12 hours, using  $N_2$  as a probe molecule at 75 K.

adsorption takes place through a process close to equilibrium conditions and, therefore, the resulting isotherm is practically free of kinetic effects.

In figure 3.7.1 are presented the adsorption isotherms for the activated samples. These  $N_2$  adsorption isotherms are characteristic of porous solids. A notorious difference between the 300°C calcinated samples and 500°C ones is evidenced by the slope of the curves. This can be attributed to the presence of different species in 300°C calcinated samples, probably due to residual organic matter (from  $Cu(acac)_2$ ), as will be discussed in the following sections. The continuous increasing tendency of these curves without a

saturation pressure is observed in the range of pressures studied. In the case of 500°C calcined samples type II isotherms are observed with a saturation pressure near 500 mmHg. For the exchanged and calcined samples, a reduction for the available volume (about 15%) is observed in concordance with the previous results reported by Sainz, *et al.*<sup>58</sup>. A different behavior was found in the CuMorO3% 400T sample tendencies do not follow the same pathways, see figure 3.7.2. We noted a considerable increase in the accessible volume after copper insertion and calcination, probably due to the copper amount employed and the calcination temperature used, conditions which apparently optimize the process, given that it is the sample that produce the higher methanol yield.

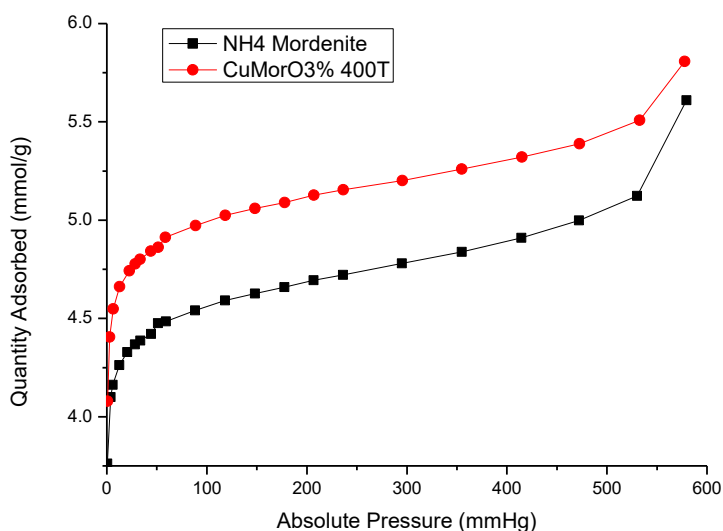


Figure 3.7.2. Adsorption isotherms of NH<sub>4</sub>-Mordenite and CuMorO<sub>3</sub>% 400T, degassed at 200°C for 12 hours, using N<sub>2</sub> as a probe molecule at 75 K.

Employing the BET (Brunauer-Emmet-Teller) method<sup>87</sup>, we estimate an approximation of pore surface area (see table 3.7.1.), interesting, the major area calculated belongs to the 3% T400 sample which corresponds to the sample that produces more methanol per catalyst gram, this behavior is expected owing to a major contact area increment the probabilities of contact between methane molecules and the active sites, producing more methanol. On the other hand, it is observed that samples calcinated at 500°C hold a mayor surface than samples calcinated at 300°C (see table 3.7.1), behavior that can be related with the existence or acetylacetonate residues present in samples calcinated at lower temperatures. The pore volume was procured by the t-plot method<sup>88</sup> (see table 3.7.1),

again, the result with the major pore volume corresponds to the CuMorO3% T400 sample, which produced more methanol than the other samples, this is expected due to mayor volumes let more methane available in the porous framework to react with the active sites, producing more methanol per gram.

A rough proposal of methanol yield approximation is based in employing the available, total micropore and mesopore volume of the material, where the active sites are located<sup>12,53,58,68</sup>, as the possible volume in which methane can be oxidized in our experiment; considering that all the methane inside the microporous/mesoporous reacts and the selectivity is 100% towards methanol. As it is only an approximation, the proposed yields should be taken with care. In table 3.7.2 the values of micromoles of methanol produced in 250 mg of each material experiment and the total methanol yield are shown, these data were obtained employing the information given by GC-MS (see table 3.4.1. and Appendix 9) and the corrected t-plot volume. For the calculation of the available volume, we consider a t-plot correction reported by Galarneau, A. *et al.*, consisting in a reduction of reported volume in a 25% approximately, in an attempt to approach to the real value of the available volume; this volume correction carry us to the methanol yield presented in table 3.7.2 (orange column). The methanol yields obtained are in a concordance with previous yields results reported by similar materials and different reactor systems<sup>53,55,97</sup>. As can be seen in table 3.7.2. the maximum yield obtained was of 96.4% corresponding to the experiment CuMorO1% 500T P2. The differences in the order in methanol production (see table 3.4.1) and yields can be owing to the non-controlled selectivity in the experiment. The results suggest that lower pressures produce higher yields.

Table 3.7.1 Resume of surface area (BET method) and volume (t-plot method) results of activated samples CuMorO5% T500, CuMorO5% T500, CuMorO3% T400, CuMorO1% T300, and CuMorO1% T300.

Copper exchanged mordenites (CuMorO)	Volume Tplot (cm <sup>3</sup> /g)	Area BET (m <sup>2</sup> /g)
1% T500	0.127088	308.35
5% T500	0.135028	306.2479
3% T400	0.148467	348.6933

1% T300	0.073862	297.4552
5% T300	0.06528	305.5101

Table 3.7.2. Methanol quantity ( $\mu\text{mol}$ ), direct and corrected, produced in 250 mg material of each experiment calculated from GC-MS and t-plot volume data; and total methanol yield obtained.

Experimental samples (250 mg)	$\mu\text{mol}$ methanol (in 250 mg)	$\mu\text{mol}$ methanol (250 mg) Vol Corr total $\mu\text{pore}$	Methanol Yield (%)
1% 300P2	1.183	1.252565938	94.4
1% 300P10	2.80375	6.262828422	44.8
1% 500P2	2.685782923	2.7868741	96.4
1% 500P10	5.183	13.93436768	37.2
5% 300P2	0.7745	1.186104363	65.3
5% 300P10	3.909	5.930520614	65.9
5% 500P2	2.115	3.122496378	67.7
5% 500P10	5.3015	15.61247873	34.0
3% 400P6	7.46	10.29981022	72.4
3% 400P6	6.18625	10.29981022	60.1
1% 500P6	1.6475	8.360620887	19.7

### 3.8 Fourier Transform Infrared Spectroscopy Analysis.

Fourier Transform Infrared spectroscopy (FTIR) is not the best analytical technique to study the copper oxide sites in mordenite because the intense broad bands of mordenite silanol groups tend to encompass the region in which the copper oxides usually appear. Furthermore, FTIR does not show information about the oxidation state directly (it does indirectly); UV-Vis spectroscopy is a better technique for this purpose. We employed IR spectroscopy to follow the changes in mordenite framework along the process (metal impregnation and calcination). Figure 3.8.1 shows the FTIR spectra of activated samples and  $\text{NH}_4$ -Mordenite. All the samples presented the typical vibrational bands of mordenite which agree with previous reports for analogous materials<sup>98</sup>. Bands attributed to Si-O stretching vibrations were found at  $1050\text{ cm}^{-1}$  and  $1240\text{ cm}^{-1}$ . Bands observed at  $918\text{ cm}^{-1}$ ,  $585\text{ cm}^{-1}$ , and  $468\text{ cm}^{-1}$  were endorsed to Al-O-Al bending vibration, coupling vibration

of Al-O and Si-O, Al-O stretching vibration and Si-O bending vibrations respectively<sup>99</sup>. Direct Copper signals (bands associated to vibrational, rotational, or electric energetic levels) are not appreciated at any spectrum, the only distinguishable changes come from the comparison between copper exchanged samples and pure ammonium mordenite. 500°C calcined samples present more changes in FTIR Spectra than samples calcined at 300°C with respect to clear NH<sub>4</sub>-Mordenite, also 500°C samples present a more defined spectra: close to 3200cm<sup>-1</sup> region it is a band associated with N-H stretching ascribed to ammonium that tends to disappear completely for the samples treated with heat. This confirms indirectly the ionic exchange between the ammonium and the copper ion from Cu(acac)<sub>2</sub>.

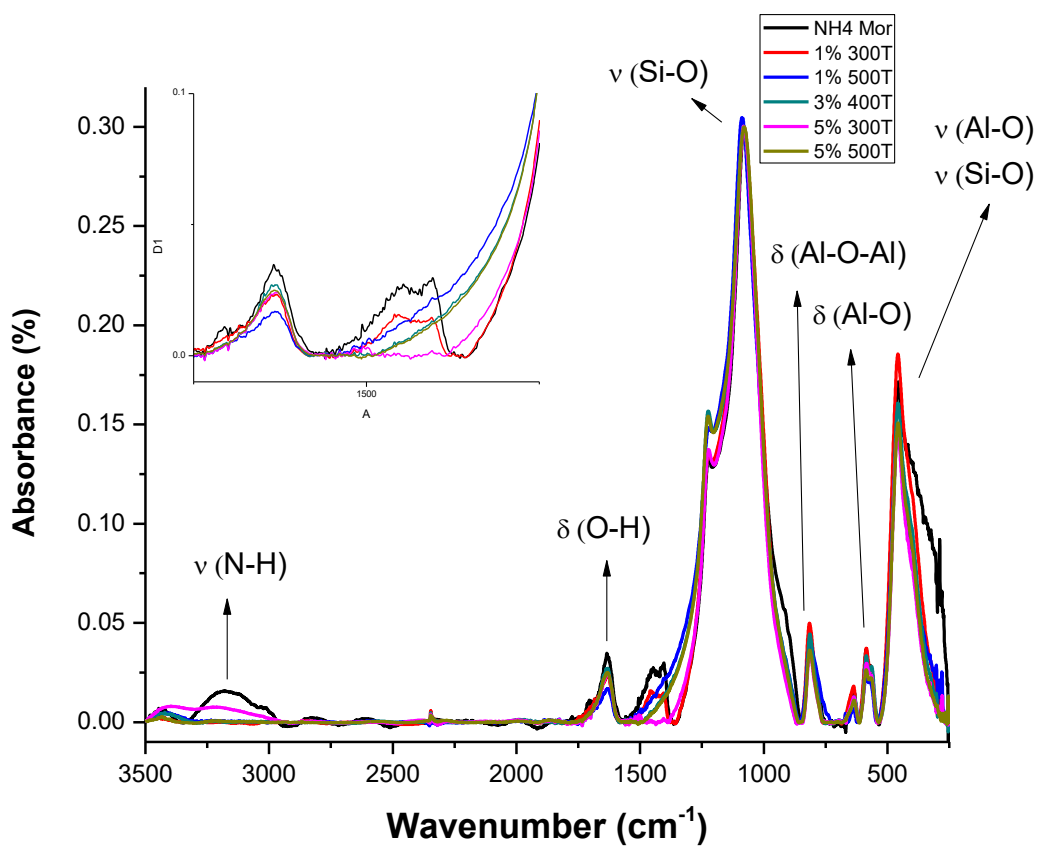


Figure 3.8.1. Bands assignment of IR spectra (1% 500T, 1% 300T, 3% 400T, 5% 500T, 1% 300T of copper exchanges samples and NH<sub>4</sub>-Mor for pure NH<sub>4</sub>-Mordenite samples). Observable changes correspond comparison between copper samples and NH<sub>4</sub>-Mordenite, and not to direct copper species.

In the  $1500\text{ cm}^{-1}$  region (left upper part zoom, figure 3.8.1) a band assigned to -OH vibrations in the pure  $\text{NH}_4$ -Mordenite spectra is observed<sup>27</sup>, this band seems to disappear after metal impregnation and calcination, suggesting the breaking of -OH bond to probably forming different species as -OM, where M (Metal) in this case correspond to Copper (Cu) atoms. In figure 3.8.2 it is displayed the FTIR spectra of Cu3t400p6b experiment sample, the one that got the best yields (see table 3.4.1). As expected, no significant changes were observed between the copper exchanged samples; only visible changes with respect to  $\text{NH}_4$ -Mordenite. For example, there is a reduction in N-H bands after copper insertion and heating process, indicating a probable ion substitution between the ammonium ions and copper ions, stabilizing the mordenite charged framework. The loss of the  $1480\text{ cm}^{-1}$  band (figure 3.8.2) for copper exchanged samples can be associated with the insertion of copper in mordenite structure forming -OCu terminals; this band is only present but diminished for the 5% 300T (pink spectrum) sample, a deficient heating transfer process could cause this<sup>27</sup>.

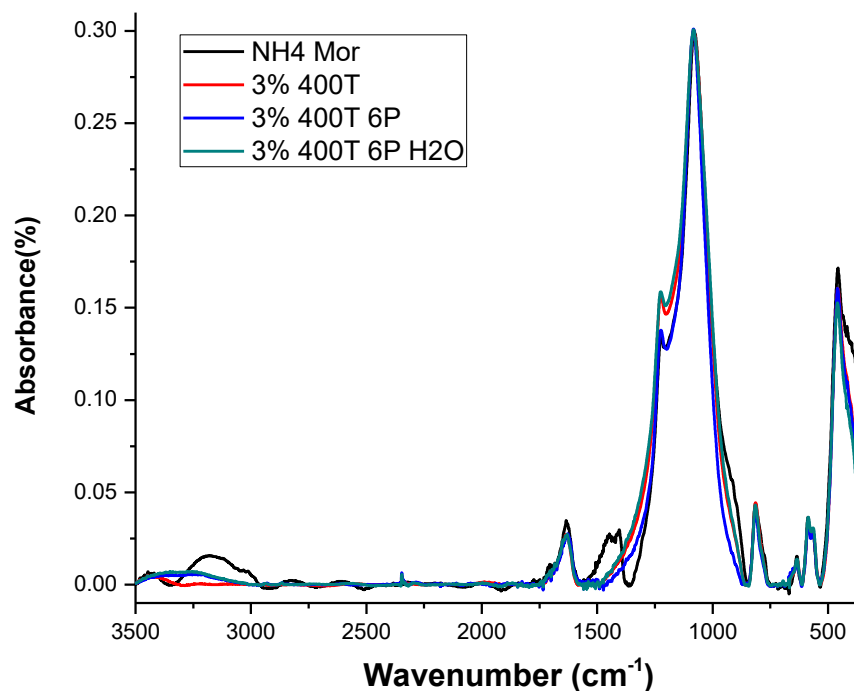


Figure 3.8.2. IR spectra of samples corresponding to the Cu3T400p6b experiment: calcined (3%400T), reacted with methane (3%400T 6P) and washed samples (3%400T H2O); and  $\text{NH}_4$ -Mordenite (NH4 Mor).

Combined with X-Ray Diffraction results, the FTIR spectra above (3%400T and NH4-Mor) show that the mordenite structure did not appreciable seems to be altered after metal impregnation, since no changes are observed in the spectra that suggest structural changes in the mordenite framework.

### 3.9 Electron Spectroscopy Analysis.

One of the main techniques to study the active sites in copper exchange zeolites is electronic spectroscopy. It helps to shed light about the oxidation state and coordination number for the exchanged copper atoms and the identity of their ligands. In this case, we applied this technique to characterize the materials, as one of the most practical approaches to detect and determine the active copper sites and their structural changes during the whole reaction cycle (figure 3.9.1). A spectrum of all samples of the entire process were taken with a UV-Vis spectrometer (equipment features in experimental section). In the region between 20000 – 30000  $\text{cm}^{-1}$  commonly appear bands associated with copper species that bind to extra-framework oxygen<sup>19,28</sup>. For analogous materials, like Copper ZSM-5 (Zeolite Socony Mobil - 5) and Copper-Mordenite (obtained by aqueous solution), as a consequence of high temperature activation, it has been reported the appearance of a broadband at 22700 $\text{cm}^{-1}$  assigned to a mono-( $\mu$ -oxo) dicopper (II) complex ( $[\text{Cu}_2(\mu\text{-O})]^{2+}$ )<sup>19,43,70</sup>. Nevertheless,, other studies reported new bands associated with different copper structures, like the trimeric copper species<sup>12,32,89</sup>, bis( $\mu$ -oxo) dicopper (III),  $\mu$ -( $\eta^2$ : $\eta^2$ ) peroxo dicopper (II) sites<sup>28,43,73</sup>, etc. These bands can appear within or out the mentioned region. The trimeric copper species appear out of 20000 – 30000  $\text{cm}^{-1}$  spectral region<sup>12</sup>. The formation of bands associated with specific copper sites is very sensible from the calcination temperature changes, in a heating process<sup>68</sup>. Two bands of two different copper sites for the same zeolite material can be present in the same spectra as reported by Samira, *et al.* However, the exact structure of the responsible species of methane to methanol conversion has not been fully understood, and a detailed understanding of the mechanism of such mordenite-catalyzed conversion is still missing. Actually, one of the current debates in studying copper exchanged zeolites is the exact configuration of the available active sites<sup>7,10,55,100,101</sup>. In this work, it was obtained the UV-

Vis Spectra of all the samples collected in the different steps of the conversion process (See figure 2.2.1 and 2.2.2, Experimental Section). Our UV-Vis work aim is to identify the nature of the copper species formed in the mordenite framework by the employed synthesis method and also determine if these species are responsible of the methane conversion.

We work with the Kubelka-Munk function  $(R) = \frac{(1-R)^2}{2R} = \frac{K}{S}$ , (See Appendix 7) to treat the data obtained. We chose the diffuse reflectance mode formalism due to the relation between the adsorption and light scattering of the high reflective porous samples, this treatment has-shown to be more sensitive with bulk copper species<sup>102</sup> and it is broadly applied for catalysis studies.

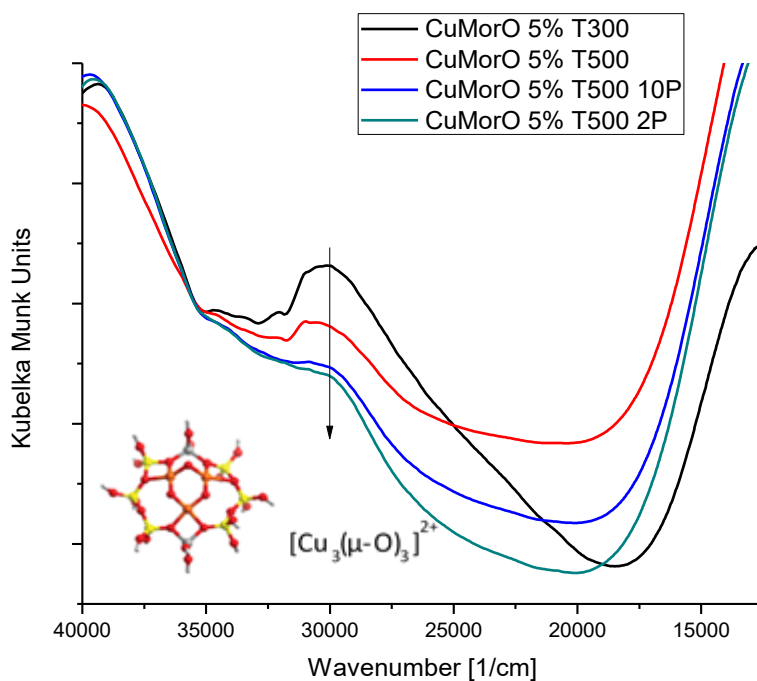


Figure 3.9.1. Bands of the activated (CuMorO5% T300, CuMorO5% T500) and reacted (CuMorO5% T500 10P, CuMorO5% T500 2P) samples with 5% wt Cu. The trimeric copper site is associated with the 31000cm<sup>-1</sup> band (Vogiatzis, K. D, et al., 2017).

Copper (II) complexes have characteristic absorption bands in the visible region related to d-d transitions<sup>58</sup> Related with their 3d<sup>9</sup> configuration. The t<sub>2g</sub> and, e<sub>g</sub> gap mainly

depends on metal coordination, its tetrahedral geometry<sup>12</sup> (see chapter 1), and ligands. From this fact, the wavenumber in which these bands appear provides information about the nature of copper active sites. Comparing the samples with the same quantity of copper-loaded in each of the three steps of the complete conversion process suggest the existence of copper species through the formation of broad bands in specific regions of the ultraviolet-visible range of electromagnetic spectra. For analogous materials, copper mordenites synthesized by aqueous solution and activated at different temperatures and medium conditions, a broader and less defined band associated with mono( $\mu$ -oxo) dicopper (II) in 22200 is reported<sup>19,74</sup>. In figure 3.9.1 it is shown a comparison between the calcined samples of 5 wt% Cu (CuMorO5% T300 and CuMorO5% T500) and the CuMorO5% T500 sample reacted with methane at 2 bar and 10 bar. Activated 5 wt% copper mordenite in figure 3.9.1, CuMorO5% T300 and CuMorO5% T500, show a defined band in the region between 30000cm<sup>-1</sup> and 31000cm<sup>-1</sup>, this observation is in accordance with the work reported by Grundner<sup>12</sup> *et al.*, in which Cu-Mordenite is activated in pure O<sub>2</sub> atmosphere at 450°C observing a formation of a new band in 30000cm<sup>-1</sup> and 31000cm<sup>-1</sup> region and the disappearance of the band at 22700cm<sup>-1</sup> related with mono(oxo) dicopper (II). According to Grundner's work this new found signal corresponds to a trimeric site<sup>12,32,89</sup> located in the 8-membered ring side pockets of mordenite framework, which is present in the spectra of the CuMorO5% T300 and CuMorO5% T500 samples (figure 3.9.1) and this band disappear for the reacted with methane samples (CuMorO5% T500 10P and CuMorO5% T500 2P spectra in figure 3.9.1.) suggesting that this signal corresponds to a reactive to methane species, having the same behavior that the reported trimeric<sup>12</sup> species; moreover, the well-defined signal observed for the same site suggests a higher homogeneity and probably the formation of unique copper active species. This absorption band is interpreted as a charge transfer O<sub>bridge</sub>→Cu transition by the formation of [Cu<sub>3</sub>( $\mu$ -O)<sub>3</sub>]<sup>2+</sup>. For Copper (I) no information is obtained from this spectra because it has 3d<sup>10</sup> electronic configuration. In the case of metallic Copper (0) cluster formation is detected as the appearance of a plasmon resonance absorption intense broad band<sup>27</sup>, seen in the 15000cm<sup>-1</sup> and 10000cm<sup>-1</sup> spectral region of

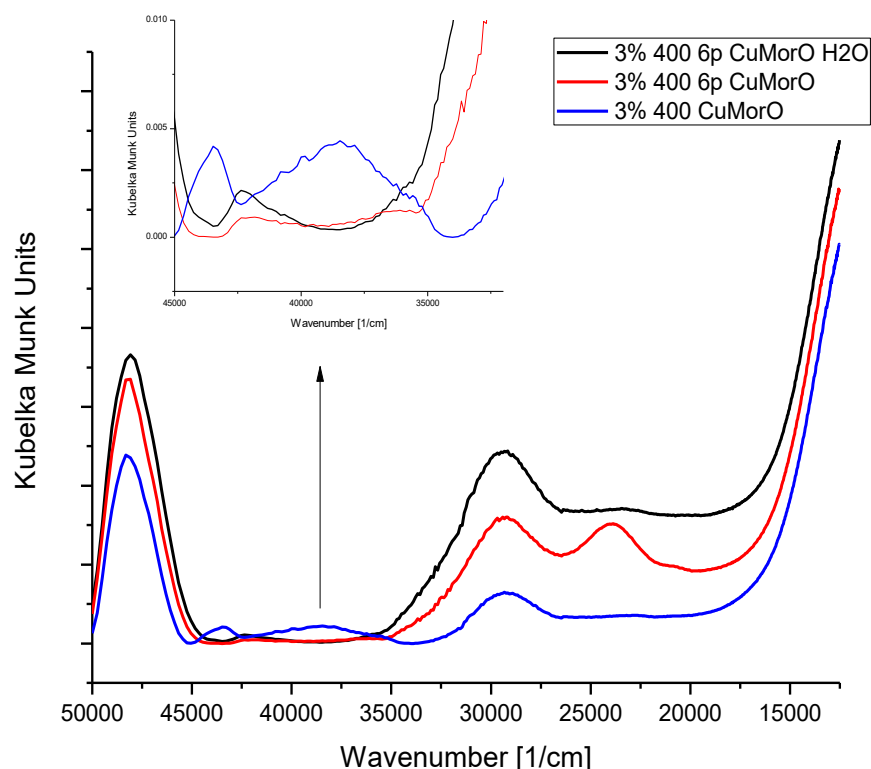


Figure 3.9.2. Three copper loaded percent samples complete cycle: activated in oxygen (3% 400 CuMorO), reacted with methane (3% 4006p CuMorO) and washed with liquid water (3% 4006p CuMorO H2O).

figure 3.9.1. Furthermore, no trace band was found that evidenced the formation of different reported copper active sites in the spectra. The broad bands centered at  $40000\text{cm}^{-1}$  are characteristic of mordenite framework<sup>89</sup> (Si-O, Al-O interactions).

The sample calcined at  $300^{\circ}\text{C}$  in figure 3.9.1 presents the most intense band, followed by the sample calcined at  $500^{\circ}\text{C}$ ; this band behavior suggests that low calcination temperatures enhance the formation of trimeric copper sites which present significant stability at room temperature. The samples reacted with methane (CuMorO5% T500 10P, CuMorO5% T500 2P) in figure 3.9.1 show a significant reduction in the band intensity, disappearing completely in the spectra of the sample CuMorO5% T500 2P, showing a better performance at low methane pressures. These results are in concordance with the methanol amounts presented in table 3.4.1 and with the global pressure analysis discussed in section 3.4.

In figure 3.9.2 is shown the complete cycle of the sample that produces the best methanol conversion performance (3% 400 CuMorO); the samples corresponding to the

Cu3t400p6b experiment. In this figure, it is observed the same band (present in  $31000\text{cm}^{-1}$ ) Shown in the 5 wt% copper cycle (figure 3.9.1) corresponding to the trimeric site, confirming that the  $400^\circ\text{C}$  calcination temperature also produces the mentioned site. It was found (figure 3.9.2) a little band located at  $38000\text{cm}^{-1}$  in Cu3t400p6a, this signal tends to increase in intensity with the calcination process and disappear with the methane reaction (and the washing process), as behavior reported by Tomkins<sup>55</sup> *et al.* This signal has not been yet reported in literature, but its existence is possible and can be related with the methane to methanol process; this is because an accurate description of the active sites in mordenites is still not entirely complete so there is the proposal of the formation of new copper species responsible for methane oxidation processes, as mentioned by Grundner<sup>12</sup>, *et al.* and Park<sup>81</sup> *et al.*

#### 4. CONCLUSIONS.

The main ionic exchange method reported for obtaining copper exchanged mordenite is by aqueous solution, in this contribution, we used the ionic exchange method by a solid-state route with satisfactory results. Solid-state synthesis pathway let us obtain homogeneous copper exchanged samples which allowing the formation of small copper clusters that derived, during the heating treatment, in the active conversion sites. The quantity of copper ion exchanged in NH<sub>4</sub>-Mordenites is close to the theoretical maximum amount allowed by stoichiometry, which in fact does not exceed 5%, this fact avoided the formation of unwanted metal copper clusters that hinder the reaction with methane; evidencing the fundamental role of stoichiometry in methanol production. The Mordenite structure is conserved once the copper ions have been exchanged, this is a very convenient result since it is possible to take advantage of the porous characteristic mordenite framework during the reaction with methane and the desorption and transport of methanol, when converted, inside the material. The employment of copper acetylacetonate as copper(II) ion precursor by mechano-synthesis worked, but it is still necessary to evaluate its yield in comparison with copper nitrate precursor. The collected experimental evidence indicates that the solid-state method followed by a heat treatment under an oxidative atmosphere (in this case air oxygen) produces the formation and stability of active-copper sites. Specifically, we found by the UV-Vis spectroscopy that the activation process (calcination procedure) results in the formation of trimeric copper sites [Cu<sub>3</sub>(μ-O)<sub>3</sub>]<sup>2+</sup>, contrary to previous reports in which mono(μ-oxo) dicopper (II) sites are responsible for the methane conversion. We identified the defined band associated with the trimeric copper species in 31000 cm<sup>-1</sup>, ascribed to a d-d transition interpreted as a charge transfer O<sub>bridge</sub>→Cu transition. We observe a minor band not reported by previous works located in the 38000cm<sup>-1</sup> centered region; ascribed to methane to methanol reactive species present in the CuMorO3% 400T sample spectra in the methane conversion cycle; more studies associated with this possible reactive species are needed. Furthermore, there exists a significant dependence of the activation temperature and quantity of copper-loaded in the nature and population of trimeric sites in copper exchanged mordenite; corroborated by the results of methanol yields.

The GC-MS statistical results showed the relation between the variables defined in the experimental design with the methanol yield in the ranges studied. We propose a non-linear model of a batch reaction that describes the experiment starting from a quadratic regression in which the calcination temperature and methane pressure have a quadratic relation. We found that the pressure behaves as expected, higher pressures mean a greater concentration and consequently a major probability of contact between methane and the active conversion sites. At lower pressures, the interaction is reduced, and consequently the amount of methanol produced, nevertheless the material still produces good methanol yields though, suggesting that methane pressure does not have a great impact in methanol production in the studied range. In the global analysis, the calcination temperature showed a linear behavior; at higher temperatures, it is obtained a higher methanol yield, but in relation with copper loaded percentage, this variable seems to have low influence in the experimental results, as suggested by its linear contribution in the model.

The central points with 3 wt% copper loaded, 400°C calcination temperature and 6 bar methane pressure conditions produced the major quantity of methanol yield (29.84  $\mu\text{mol/g}$ ), open new questions about the optimization of the methane to methanol batch reaction conditions.

Thermogravimetric analysis evidenced a higher temperature for acetylacetonate elimination compared with its decomposition temperature; this explains the conservation of organic matter in samples calcined at 300°C. The absorption analysis shows a great dependence of calcination temperature in the porosity of materials, showing a notorious increment in the volume available for the sample CuMorO3% 400T (the one with the highest methane yield), this behavior was not expected since copper insertion should reduce absorption nitrogen performance, this result suggests a major population of active copper sites according to its adsorption hysteresis. Although the obtained methanol yields were generally low in comparison with the continuous flow reaction conditions, the obtained results reported in this contribution shed light of different experimental methanol conversion methods and motivates further studies.

## 5. REFERENCES.

1. Shamsul, N. S., Kamarudin, S. K., Rahman, N. A. & Kofli, N. T. An overview on the production of bio-methanol as potential renewable energy. *Renew. Sustain. Energy Rev.* **33**, 578–588 (2014).
2. WMO, Water, W. C. & WMO. Wmo Greenhouse Gas. *World Meteorol. Organ. Bull.* 1–4 (2017). doi:ISSN 2078-0796
3. Wade, L. G. J. *Química Orgánica*. (Pearson-Prentice Hall, 2004).
4. Yvon-Durocher, G. *et al.* Methane fluxes show consistent temperature dependence across microbial to ecosystem scales. *Nature* **507**, 488 (2014).
5. Meunier, M., Quirke, N. & Binesti, D. The Calculation of the Electron Affinity of Atoms and Molecules. *Mol. Simul.* **23**, 109–125 (1999).
6. Dinh, K. T. *et al.* Viewpoint on the Partial Oxidation of Methane to Methanol Using Cu- and Fe-Exchanged Zeolites. *ACS Catal.* **8**, 8306–8313 (2018).
7. Tomkins, P., Ranocchiari, M. & van Bokhoven, J. A. Direct Conversion of Methane to Methanol under Mild Conditions over Cu-Zeolites and beyond. *Acc. Chem. Res.* **50**, 418–425 (2017).
8. World Energy Statistics 2018. (2018). doi:10.1787/world\_energy\_stats-2018-en
9. Olivos-Suarez, A. I. *et al.* Strategies for the Direct Catalytic Valorization of Methane Using Heterogeneous Catalysis: Challenges and Opportunities. *ACS Catal.* **6**, 2965–2981 (2016).
10. Hammond, C., Conrad, S. & Hermans, I. Oxidative methane upgrading. *ChemSusChem* **5**, 1668–1686 (2012).
11. Mills, G. *Status and Future Opportunities for Conversion of Synthesis Gas to Liquid Energy Fuels: Final Report*. National Renewable Energy Laboratory (1993).
12. Grundner, S. *et al.* Single-site trinuclear copper oxygen clusters in mordenite for selective conversion of methane to methanol. *Nat. Commun.* **6**, 7546 (2015).
13. Choudhary, T. V., Aksoylu, E. & Wayne Goodman, D. Nonoxidative Activation of Methane. *Catal. Rev.* **45**, 151–203 (2003).

14. Soorholtz, M. *et al.* Direct methane oxidation over Pt-modified nitrogen-doped carbons. *Chem. Commun.* **49**, 240–242 (2013).
15. Guo, Z. *et al.* Recent advances in heterogeneous selective oxidation catalysis for sustainable chemistry. *Chem. Soc. Rev.* **43**, 3480–3524 (2014).
16. Arutyunov, V. Chapter 2 - Oxidation Products. in (ed. Arutyunov, V. B. T.-D. M. to M.) 5–28 (Elsevier, 2014). doi:<https://doi.org/10.1016/B978-0-444-63253-1.00002-7>
17. Achmad, F., Kamarudin, S. K., Daud, W. R. W. & Majlan, E. H. Passive direct methanol fuel cells for portable electronic devices. *Appl. Energy* **88**, 1681–1689 (2011).
18. Zakaria, Z. & Kamarudin, S. K. Direct conversion technologies of methane to methanol: An overview. *Renew. Sustain. Energy Rev.* **65**, 250–261 (2016).
19. Wulfers, M. J., Teketel, S., Ipek, B. & Lobo, R. F. Conversion of methane to methanol on copper-containing small-pore zeolites and zeotypes. *Chem. Commun.* **51**, 4447–4450 (2015).
20. Tinberg, C. E. & Lippard, S. J. Dioxygen activation in soluble methane monooxygenase. *Acc. Chem. Res.* **44**, 280–288 (2011).
21. Colby, J., Stirling, D. I. & Dalton, H. *The soluble methane mono-oxygenase of Methylococcus capsulatus (Bath). Its ability to oxygenate n-alkanes, n-alkenes, ethers, and alicyclic, aromatic and heterocyclic compounds.* *The Biochemical journal* **165**, (1977).
22. Snyder, B. E. R., Bols, M. L., Schoonheydt, R. A., Sels, B. F. & Solomon, E. I. Iron and Copper Active Sites in Zeolites and Their Correlation to Metalloenzymes. *Chem. Rev.* **118**, 2718–2768 (2018).
23. Rosenzweig, A. C., Frederick, C. A., Lippard, S. J. & Nordlund, P. Crystal structure of a bacterial non-haem iron hydroxylase that catalyses the biological oxidation of methane. *Nature* **366**, 537–543 (1993).
24. Bordeaux, M., Galarneau, A. & Drone, J. Catalytic, mild, and selective oxyfunctionalization of linear alkanes: Current challenges. *Angew. Chemie - Int. Ed.* **51**, 10712–10723 (2012).
25. Beznis, N. V, Weckhuysen, B. M. & Bitter, J. H. Partial Oxidation of Methane Over Co-

- ZSM-5: Tuning the Oxygenate Selectivity by Altering the Preparation Route. *Catal. Letters* **136**, 52–56 (2010).
26. Starokon, E. V, Parfenov, M. V, Pirutko, L. V, Abornev, S. I. & Panov, G. I. Room-Temperature Oxidation of Methane by  $\alpha$ -Oxygen and Extraction of Products from the FeZSM-5 Surface. *J. Phys. Chem. C* **115**, 2155–2161 (2011).
  27. Priya, S. S., Selvakannan, P. R., Chary, K. V. R., Kantam, M. L. & Bhargava, S. K. Solvent-free microwave-assisted synthesis of solketal from glycerol using transition metal ions promoted mordenite solid acid catalysts. *Mol. Catal.* **434**, 184–193 (2017).
  28. Smeets, P. J. *et al.* Oxygen Precursor to the Reactive Intermediate in Methanol Synthesis by Cu-ZSM-5. *J. Am. Chem. Soc.* **132**, 14736–14738 (2010).
  29. Alvarez-Galvan, M. C. *et al.* Direct methane conversion routes to chemicals and fuels. *Catal. Today* **171**, 15–23 (2011).
  30. Tabata, K. *et al.* Activation of methane by oxygen and nitrogen oxides. *Catal. Rev.* **44**, 1–58 (2002).
  31. Holmen, A. Direct conversion of methane to fuels and chemicals. *Catal. Today* **142**, 2–8 (2009).
  32. Vogiatzis, K. D., Li, G., Hensen, E. J. M., Gagliardi, L. & Pidko, E. A. Electronic Structure of the [Cu(3)( $\mu$ -O)(3)](2+) Cluster in Mordenite Zeolite and Its Effects on the Methane to Methanol Oxidation. *J. Phys. Chem. C. Nanomater. Interfaces* **121**, 22295–22302 (2017).
  33. Zhang, X., He, D., Zhang, Q., Xu, B.-Q. & Zhu, Q. CATALYTIC CONVERSION OF METHANE TO METHANOL OVER LANTHANUM-COBALT-OXIDE SUPPORTED MOLYBDENUM BASED CATALYSTS. (2019).
  34. Raja, R. & Ratnasamy, P. Direct conversion of methane to methanol. *Appl. Catal. A Gen.* **158**, L7–L15 (1997).
  35. Starokon, E. V *et al.* Oxidation of methane to methanol on the surface of FeZSM-5 zeolite. *J. Catal.* **300**, 47–54 (2013).
  36. Krisnandi, Y. K. *et al.* Partial Oxidation of Methane to Methanol over Heterogeneous Catalyst Co/ZSM-5. *Procedia Chem.* **14**, 508–515 (2015).

37. Xu, J. *et al.* Continuous selective oxidation of methane to methanol over Cu- and Fe-modified ZSM-5 catalysts in a flow reactor. *Catal. Today* **270**, 93–100 (2016).
38. Khirsariya, P. & Mewada, R. K. Single Step Oxidation of Methane to Methanol—Towards Better Understanding. *Procedia Eng.* **51**, 409–415 (2013).
39. Periana, R. A. *et al.* Platinum Catalysts for the High-Yield Oxidation of Methane to a Methanol Derivative. *Science (80-. )*. **280**, 560 LP – 564 (1998).
40. Periana, R. A. *et al.* A Mercury-Catalyzed, High-Yield System for the Oxidation of Methane to Methanol. *Science (80-. )*. **259**, 340 LP – 343 (1993).
41. Shilov, A. E. & Shul'pin, G. B. Activation of C–H Bonds by Metal Complexes. *Chem. Rev.* **97**, 2879–2932 (1997).
42. Michalkiewicz, B. *Kinetics of Partial Methane Oxidation Process over the Fe-ZSM-5 Catalysts. Chemical Papers* **59**, (2005).
43. Groothaert, M. H., Smeets, P. J., Sels, B. F., Jacobs, P. A. & Schoonheydt, R. A. Selective Oxidation of Methane by the Bis( $\mu$ -oxo)dicopper Core Stabilized on ZSM-5 and Mordenite Zeolites. *J. Am. Chem. Soc.* **127**, 1394–1395 (2005).
44. Verma, S. S. To study the direct transformation of methane into methanol in the lower temperature range. *Energy Convers. Manag.* **43**, 1999–2008 (2002).
45. Razumovsky, S. D. *et al.* Effect of immobilization on the main dynamic characteristics of the enzymatic oxidation of methane to methanol by bacteria *Methylosinus sporium* B-2121. *Russ. Chem. Bull.* **57**, 1633–1636 (2008).
46. Michalkiewicz, B. Partial oxidation of methane to formaldehyde and methanol using molecular oxygen over Fe-ZSM-5. *Appl. Catal. A Gen.* **277**, 147–153 (2004).
47. Taylor, C. E. & Noceti, R. P. New developments in the photocatalytic conversion of methane to methanol. *Catal. Today* **55**, 259–267 (2000).
48. Reddy, P. V. L., Kim, K.-H. & Song, H. Emerging green chemical technologies for the conversion of CH<sub>4</sub> to value added products. *Renew. Sustain. Energy Rev.* **24**, 578–585 (2013).
49. Lee, B. & Hibino, T. Efficient and selective formation of methanol from methane in a fuel cell-type reactor. *J. Catal.* **279**, 233–240 (2011).

50. Ma, M. *et al.* Ultrahigh Electrocatalytic Conversion of Methane at Room Temperature. *Adv. Sci.* **4**, 1700379 (2017).
51. Bozbag, S. E. *et al.* Methane to methanol over copper mordenite: yield improvement through multiple cycles and different synthesis techniques. *Catal. Sci. Technol.* **6**, 5011–5022 (2016).
52. Narsimhan, K., Iyoki, K., Dinh, K. & Román-Leshkov, Y. Catalytic Oxidation of Methane into Methanol over Copper-Exchanged Zeolites with Oxygen at Low Temperature. *ACS Cent. Sci.* **2**, 424–429 (2016).
53. Kulkarni, A. R., Zhao, Z.-J., Siahrostami, S., Nørskov, J. K. & Studt, F. Cation-exchanged zeolites for the selective oxidation of methane to methanol. *Catal. Sci. Technol.* **8**, 114–123 (2018).
54. Lee, S. J., McCormick, M. S., Lippard, S. J. & Cho, U.-S. Control of substrate access to the active site in methane monooxygenase. *Nature* **494**, 380 (2013).
55. Tomkins, P. *et al.* Isothermal Cyclic Conversion of Methane into Methanol over Copper-Exchanged Zeolite at Low Temperature. *Angew. Chemie - Int. Ed.* **55**, 5467–5471 (2016).
56. Tomkins, P. *et al.* Increasing the activity of copper exchanged mordenite in the direct isothermal conversion of methane to methanol by Pt and Pd doping. *Chem. Sci.* **10**, 167–171 (2019).
57. Priya, S. S., Selvakannan, P. R., Chary, K. V. R., Kantam, M. L. & Bhargava, S. K. Solvent-free microwave-assisted synthesis of solketal from glycerol using transition metal ions promoted mordenite solid acid catalysts. *Mol. Catal.* **434**, 184–193 (2017).
58. Sainz-Vidal, A., Balmaseda, J., Lartundo-Rojas, L. & Reguera, E. Preparation of Cu-mordenite by ionic exchange reaction under milling: A favorable route to form the mono-( $\mu$ -oxo) dicopper active species. *Microporous Mesoporous Mater.* **185**, 113–120 (2014).
59. Hammond, C. *et al.* Direct Catalytic Conversion of Methane to Methanol in an Aqueous Medium by using Copper-Promoted Fe-ZSM-5. *Angew. Chemie Int. Ed.* **51**, 5129–5133 (2012).
60. Banerjee, R., Proshlyakov, Y., Lipscomb, J. D. & Proshlyakov, D. A. Structure of the key species in the enzymatic oxidation of methane to methanol. *Nature* **518**, 431 (2015).

61. Ono, K. & Erhard, A. Ullmann's Encyclopedia of Industrial Chemistry. in (2011). doi:10.1002/14356007.o17\_o02
62. Dyer, A. D. L. Bish & D. W. Ming (Editors) Natural Zeolites : Occurrences, Properties, Applications. Reviews in Mineralogy and Geochemistry, 45. 2001, 662 pp. Price US\$32. ISBN 1529-6466. *Clay Miner.* **37**, 733 (2002).
63. Oord, R., Schmidt, J. E. & Weckhuysen, B. M. Methane-to-methanol conversion over zeolite Cu-SSZ-13, and its comparison with the selective catalytic reduction of NO<sub>x</sub> with NH<sub>3</sub>. *Catal. Sci. Technol.* **8**, 1028–1038 (2018).
64. Ellis, L., Alexander, R. & Kagi, R. I. Separation of petroleum hydrocarbons using dealuminated mordenite molecular sieve—II. Alkyl-naphthalenes and alkylphenanthrenes. *Org. Geochem.* **21**, 849–855 (1994).
65. Veefkind, V. A., Smidt, M. L. & Lercher, J. A. On the role of strength and location of Brønsted acid sites for ethylamine synthesis on mordenite catalysts. *Appl. Catal. A Gen.* **194–195**, 319–332 (2000).
66. Townsend, R. P. & Coker, E. N. Chapter 11 Ion exchange in zeolites. in *Introduction to Zeolite Science and Practice* (eds. van Bekkum, H., Flanigen, E. M., Jacobs, P. A. & Jansen, J. C. B. T.-S. in S. S. and C.) **137**, 467–524 (Elsevier, 2001).
67. Simon, Y. C. & Craig, S. L. *Mechanochemistry in Materials*. (The Royal Society of Chemistry, 2018). doi:10.1039/9781782623885
68. Le, H. V *et al.* Solid-State Ion-Exchanged Cu/Mordenite Catalysts for the Direct Conversion of Methane to Methanol. *ACS Catal.* **7**, 1403–1412 (2017).
69. Echevarría, F. *et al.* Hydrothermal recrystallization of transition metal nitroprussides. Formation of the most stable phases. *Journal of Solid State Chemistry* **258**, (2017).
70. Sheppard, T., Hamill, C. D., Goguet, A., Rooney, D. W. & Thompson, J. M. A low temperature, isothermal gas-phase system for conversion of methane to methanol over Cu-ZSM-5. *Chem. Commun.* **50**, 11053–11055 (2014).
71. Grundner, S., Luo, W., Sanchez-Sanchez, M. & Lercher, J. A. Synthesis of single-site copper catalysts for methane partial oxidation. *Chem. Commun.* **52**, (2016).
72. Mahyuddin, M. H., Staykov, A., Shiota, Y. & Yoshizawa, K. Direct Conversion of

- Methane to Methanol by Metal-Exchanged ZSM-5 Zeolite (Metal = Fe, Co, Ni, Cu). *ACS Catal.* **6**, 8321–8331 (2016).
73. Woertink, J. S. *et al.* A  $[\text{Cu}_2\text{O}]_2$  core in Cu-ZSM-5, the active site in the oxidation of methane to methanol. *Proc. Natl. Acad. Sci.* **106**, 18908 LP – 18913 (2009).
74. Alayon, E. M., Nachtegaal, M., Ranocchiari, M. & van Bokhoven, J. A. Catalytic conversion of methane to methanol over Cu–mordenite. *Chem. Commun.* **48**, 404–406 (2012).
75. Chan, S. I. *et al.* Efficient Oxidation of Methane to Methanol by Dioxygen Mediated by Tricopper Clusters. *Angew. Chemie Int. Ed.* **52**, 3731–3735 (2013).
76. Mahyuddin, M. H., Tanaka, T., Shiota, Y., Staykov, A. & Yoshizawa, K. Methane Partial Oxidation over  $[\text{Cu}_2(\mu\text{-O})]_2^+$  and  $[\text{Cu}_3(\mu\text{-O})_3]_2^+$  Active Species in Large-Pore Zeolites. *ACS Catal.* **8**, 1500–1509 (2018).
77. Grundner, S., Luo, W., Sanchez-Sanchez, M. & Lercher, J. A. Synthesis of single-site copper catalysts for methane partial oxidation. *Chem. Commun.* **52**, 2553–2556 (2016).
78. Dietl, N., Schlangen, M. & Schwarz, H. Thermal Hydrogen-Atom Transfer from Methane: The Role of Radicals and Spin States in Oxo-Cluster Chemistry. *Angew. Chemie Int. Ed.* **51**, 5544–5555 (2012).
79. Perkampus, H.-H. *UV-VIS spectroscopy and its applications. Choice Reviews Online* **30**, (Springer, 2013).
80. Stuart, B. H. *Infrared Spectroscopy: Fundamentals and Applications.* (Wiley, 2004).
81. Park, M. B., Ahn, S. H., Mansouri, A., Ranocchiari, M. & van Bokhoven, J. A. Comparative Study of Diverse Copper Zeolites for the Conversion of Methane into Methanol. *ChemCatChem* **9**, 3705–3713 (2017).
82. Roessler, M. M. & Salvadori, E. Principles and applications of EPR spectroscopy in the chemical sciences. *Chem. Soc. Rev.* **47**, 2534–2553 (2018).
83. Cammack, R. EPR, Methods. in (ed. Lindon, J. C. B. T.-E. of S. and S.) 457–469 (Elsevier, 1999). doi:<https://doi.org/10.1006/rwsp.2000.0077>
84. Schosseler, P. Basic Concepts of EPR. *ETH Zürich* Available at:

<https://epr.ethz.ch/education/basic-concepts-of-epr.html>. (Accessed: 10th June 2019)

85. Moore, E. A. & Smart, L. E. *Solid State Chemistry: An Introduction*. (CRC Press, 2012).
86. Ismail, A. F., Khulbe, K. C. & Matsuura, T. *Gas separation membranes: Polymeric and inorganic. Gas Separation Membranes: Polymeric and Inorganic* (2015).  
doi:10.1007/978-3-319-01095-3
87. Rouquerol, J., Rouquerol, F., Llewellyn, P., Maurin, G. & Sing, K. *Adsorption by Powders and Porous Solids*. (Academic Press, 2013).
88. Galarneau, A., Villemot, F., Rodriguez, J., Fajula, F. & Coasne, B. Validity of the t-plot Method to Assess Microporosity in Hierarchical Micro/Mesoporous Materials. *Langmuir* **30**, 13266–13274 (2014).
89. Vanelderen, P. *et al.* Spectroscopic Definition of the Copper Active Sites in Mordenite: Selective Methane Oxidation. *J. Am. Chem. Soc.* **137**, 6383–6392 (2015).
90. Benesi, H. A. Relationship between catalytic activity and nature of acidity of the crystalline zeolites, mordenite and Y faujasite. *J. Catal.* **8**, 368–374 (1967).
91. González-Velasco, J., Pereda-Ayo, B., De La Torre, U., Urrutxua, M. & Lopez-Fonseca, R. *Coupled NSR-SCR Systems for NO<sub>x</sub> Removal in Light-Duty Vehicles*. *ChemCatChem* (2018). doi:10.1002/cctc.201800392
92. Sakizci, M. & Tanriverdi, L. *Influence of acid and heavy metal cation exchange treatments on methane adsorption properties of mordenite*. *TURKISH JOURNAL OF CHEMISTRY* **39**, (2015).
93. Majid, sheikh, Mir, M. & Mir, J. M. *Nitrate and phosphate sorption efficiency of mordenite versus zeolite-A at the convergence of experimental and density functionalized evaluation*. *Journal of the Chinese Advanced Materials Society* (2018).  
doi:10.1080/22243682.2018.1542342
94. Sushkevich, V. L., Palagin, D. & van Bokhoven, J. A. The Effect of the Active-Site Structure on the Activity of Copper Mordenite in the Aerobic and Anaerobic Conversion of Methane into Methanol. *Angew. Chemie Int. Ed.* **57**, 8906–8910 (2018).
95. Eder, F., Stockenhuber, M. & Lercher, J. A. Brønsted Acid Site and Pore Controlled Siting of Alkane Sorption in Acidic Molecular Sieves. *J. Phys. Chem. B* **101**, 5414–5419

(1997).

96. Hackett, C. & Hammond, K. D. Simulating the effect of the quadrupole moment on the adsorption of nitrogen in siliceous zeolites. *Microporous Mesoporous Mater.* **263**, 231–235 (2018).
97. Sushkevich, V. L. & van Bokhoven, J. A. Effect of Brønsted acid sites on the direct conversion of methane into methanol over copper-exchanged mordenite. *Catal. Sci. Technol.* **8**, 4141–4150 (2018).
98. Lónyi, F., Kovács, A., Szegedi, Á. & Valyon, J. Activation of Hydrogen and Hexane over Pt,H-Mordenite Hydroisomerization Catalysts. *J. Phys. Chem. C* **113**, 10527–10540 (2009).
99. Bevilacqua, M. & Busca, G. A study of the localization and accessibility of Brønsted and Lewis acid sites of H-mordenite through the FT-IR spectroscopy of adsorbed branched nitriles. *Catal. Commun.* **3**, 497–502 (2002).
100. Dyballa, M. *et al.* On How Copper Mordenite Properties Govern the Framework Stability and Activity in the Methane-to-Methanol Conversion. *ACS Catal.* **9**, 365–375 (2019).
101. Pappas, D. K. *et al.* Methane to Methanol: Structure–Activity Relationships for Cu-CHA. *J. Am. Chem. Soc.* **139**, 14961–14975 (2017).
102. Nobbs, J. H. Kubelka—Munk Theory and the Prediction of Reflectance. *Rev. Prog. Color. Relat. Top.* **15**, 66–75 (1985).

## 6. APPENDIX

Appendix 1.

Employing the empirical formula of mordenite found in the following link, where Na and K ions substitute the ammonium ion:

<http://www.webmineral.com/Mordenite.shtml#.XMd4DSJTK00>



Na 1.1

K 0.1

This 1.2 monovalent atoms (Na and K) correspond to 0.6 Copper divalent atoms.

Cu 0.6

Ca 0.5

Al 2.2

Si 9.8

O 24

H<sub>2</sub>O 5.9

We made the calculation of the maximum amount of Copper capable of substituting the monovalent ions in the mordenite, as follows:

Element	Molecular Weight	Contribution per atom to the molecule	Weight Contribution	Maximus % of copper exchanged
Cu	63.546	0.6	38.1276	4.31776508
Ca	40.08	0.5	20.04	
Al	26.98154	2.2	59.359388	
Si	28.0855	9.8	275.2379	
O	15.9994	24	383.9856	
H	1.0079	11.8	11.89322	
O	15.9994	5.9	94.39646	

			883.040168
--	--	--	------------

The maximum 4.31% wt copper can be exchanged in mordenite, with the empirical formula described above. Approximate to the value reported of 4.5% wt Cu<sup>61</sup>.

### Appendix 2.

Calculation of the quantity of Cu(acac)<sub>2</sub> added to 900mg of NH<sub>4</sub>-Mordenite to obtain 1% wt, 3% wt and 5% wt of copper, considering  $M_{atomCu}=63.56$ ,  $MM_{AcAcetCu}=261.76$ ,  $m_{mordenita}=900\text{mg}$  as known parameters and  $m_{AcAcetCu}$  as unknown quantity. These quantities were verified by using ICP-OES technique.

$$\%Cu = \frac{m_{AcAcetCu} \times \frac{M_{atomCu}}{MM_{AcAcetCu}}}{m_{mordenita} + m_{AcAcetCu}} \times 100$$

$$\%Cu \times (m_{mordenita} + m_{AcAcetCu}) = m_{AcAcetCu} \times \frac{M_{atomCu}}{MM_{AcAcetCu}} \times 100$$

$$\%Cu \times m_{mordenita} + \%Cu \times m_{AcAcetCu} = m_{AcAcetCu} \times \frac{M_{atomCu} \times 100}{MM_{AcAcetCu}}$$

$$\%Cu \times m_{mordenita} \times \frac{MM_{AcAcetCu}}{M_{atomCu} \times 100} + \%Cu \times m_{AcAcetCu} \times \frac{MM_{AcAcetCu}}{M_{atomCu} \times 100} = m_{AcAcetCu}$$

$$\%Cu \times m_{mordenita} \times \frac{MM_{AcAcetCu}}{M_{atomCu} \times 100} = m_{AcAcetCu} - \%Cu \times m_{AcAcetCu} \times \frac{MM_{AcAcetCu}}{M_{atomCu} \times 100} = m_{AcAcetCu} \left( 1 - \%Cu \times \frac{MM_{AcAcetCu}}{M_{atomCu} \times 100} \right)$$

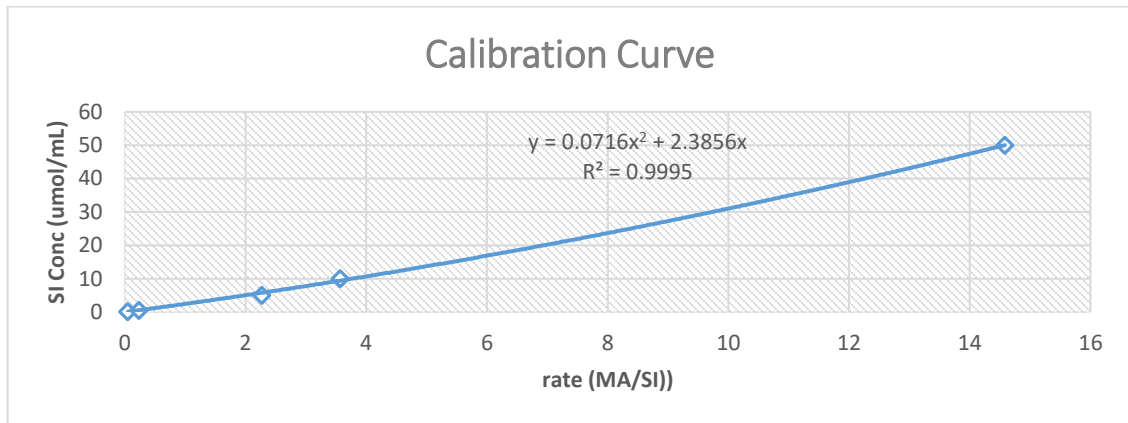
$$m_{AcAcetCu} = \frac{\%Cu \times m_{mordenita} \times \frac{MM_{AcAcetCu}}{M_{atomCu} \times 100}}{\left( 1 - \%Cu \times \frac{MM_{AcAcetCu}}{M_{atomCu} \times 100} \right)} = \frac{\%Cu \times 900 \times \frac{261.76}{63.56 \times 100}}{\left( 1 - \%Cu \times \frac{261.76}{63.56 \times 100} \right)}$$

### Appendix 3.

Chromatographic Calibration Curve to quantitate the amount of methanol obtained in each of the experiments, described in chapter 2.

Standard (SI) Concentration	Methanol Area	SI Area	Area
--------------------------------	------------------	---------	------

( $\mu\text{L}/\text{mL}$ )			
0.1	15737	312456	0.05036549
0.5	100757.49	434386.273	0.23195367
1	50203.279	303701.051	
5	861109.774	378939.853	2.27241808
10	1869045.08	523414.476	3.57087005
50	6020660.55	412896.212	14.581535



Appendix 4.

ICP-OES Copper weight percentage Data.

Sample ID	Elem	Wavelength	Int (Corr)	Reported Conc (Calib)	Reported Conc (Samp)	Calib Units
0	Cu	327.393	4909.02826	[0.00]		mg/mL
0.05	Cu	327.393	8637099.97	[0.05]		mg/mL
0.1	Cu	327.393	16921440.1	[0.1]		mg/mL
0.3	Cu	327.393	51975642.4	[0.3]		mg/mL
0.5	Cu	327.393	87776189.9	[0.5]		mg/mL
0.7	Cu	327.393		[0.7]		mg/mL
1% Cu wt d10	Cu	327.393	1696948.94	0.011	0.011	mg/mL
3% Cu wt d10	Cu	327.393	5099813.9	0.031	0.031	mg/mL
5% Cu wt d10	Cu	327.393	8563091.75	0.05	0.05	mg/mL

1% Cu wt	Cu	327.393	16041230.3	0.093	0.093	mg/mL
3% Cu wt	Cu	327.393	50470840.8	0.289	0.289	mg/mL
5% Cu wt	Cu	327.393	84152479.8	0.481	0.481	mg/mL

Appendix 5.

Table 1. Polynomial regression model, main effect analysis.

Effect	umol/g Param.	umol/g Std.Err	umol/g t	umol/g p	-95.00% Cnf.Lmt	+95.00% Cnf.Lmt	umol/g Beta (β)
Intercept	27.2926	2.455444	11.11513	0.000103	20.9807	33.6045	
Cat	-0.6961	1.227722	-0.56695	0.595252	-3.8520	2.4599	- 0.07503
Cat^2	- 25.5185	4.593715	-5.55508	0.002599	- 37.3270	-13.7100	- 1.17882
Tcal	4.1258	1.227722	3.36050	0.020097	0.9698	7.2817	0.44471
Tcal^2	0.0000						
P	4.4013	1.227722	3.58494	0.015792	1.2453	7.5573	0.44955
P^2	11.0219	4.071894	2.70683	0.042436	0.5548	21.4891	0.58792

Table 2. Comparison between observed results from the experiment (see chapter 2 and chapter 3) and the predicted ones by using a nonlinear model.

$$Yield = A + B * \%Cu + C * (\%Cu)^2 + L * Tcal + Q * P + R * P^2$$

<b>Dependent Variable: Yield (umol/g)</b>			
<b>Samples</b>	<b>Observed</b>	<b>Predicted</b>	<b>Residuals</b>
cu1t300p10	11.21507	13.76764	-2.55257
cu1t300p2	4.73229	4.96503	-0.23274
cu1t500p10	20.73241	22.01917	-1.28676
cu1t500p2	17.28864	13.21656	4.07208
cu5t300p10	15.63592	12.37553	3.26039
cu5t300p2	3.09784	3.57292	-0.47507
cu5t500p10	21.20600	20.62705	0.57895
cu5t500p2	8.46018	11.82445	-3.36426
cu3t400p6a	24.74549	27.29259	-2.54709
cu3t400p6b	29.83968	27.29259	2.54709

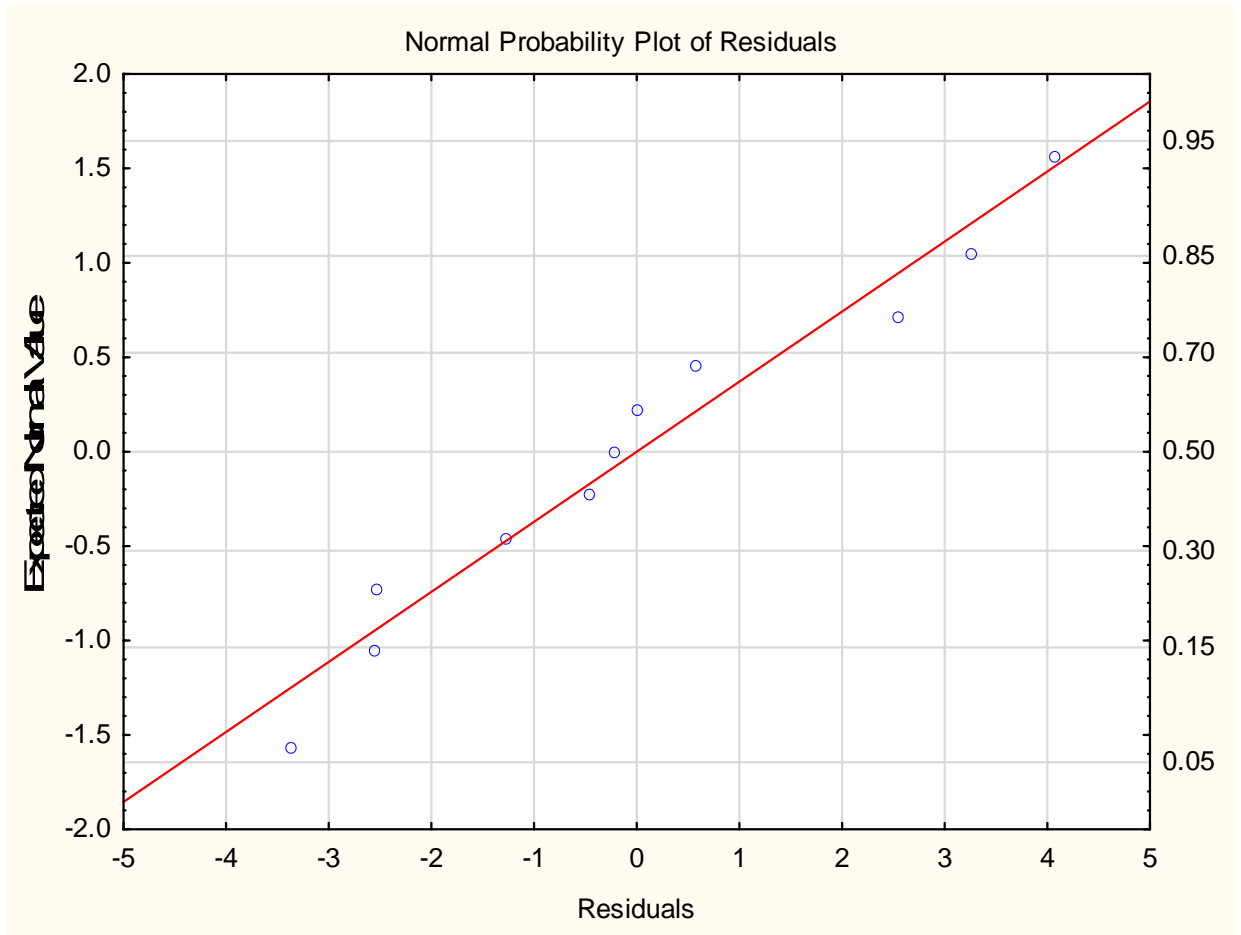


Figure 1. Expected normal values against residuals obtained with the nonlinear model.

The redline approximation suggests a better description of experiments.

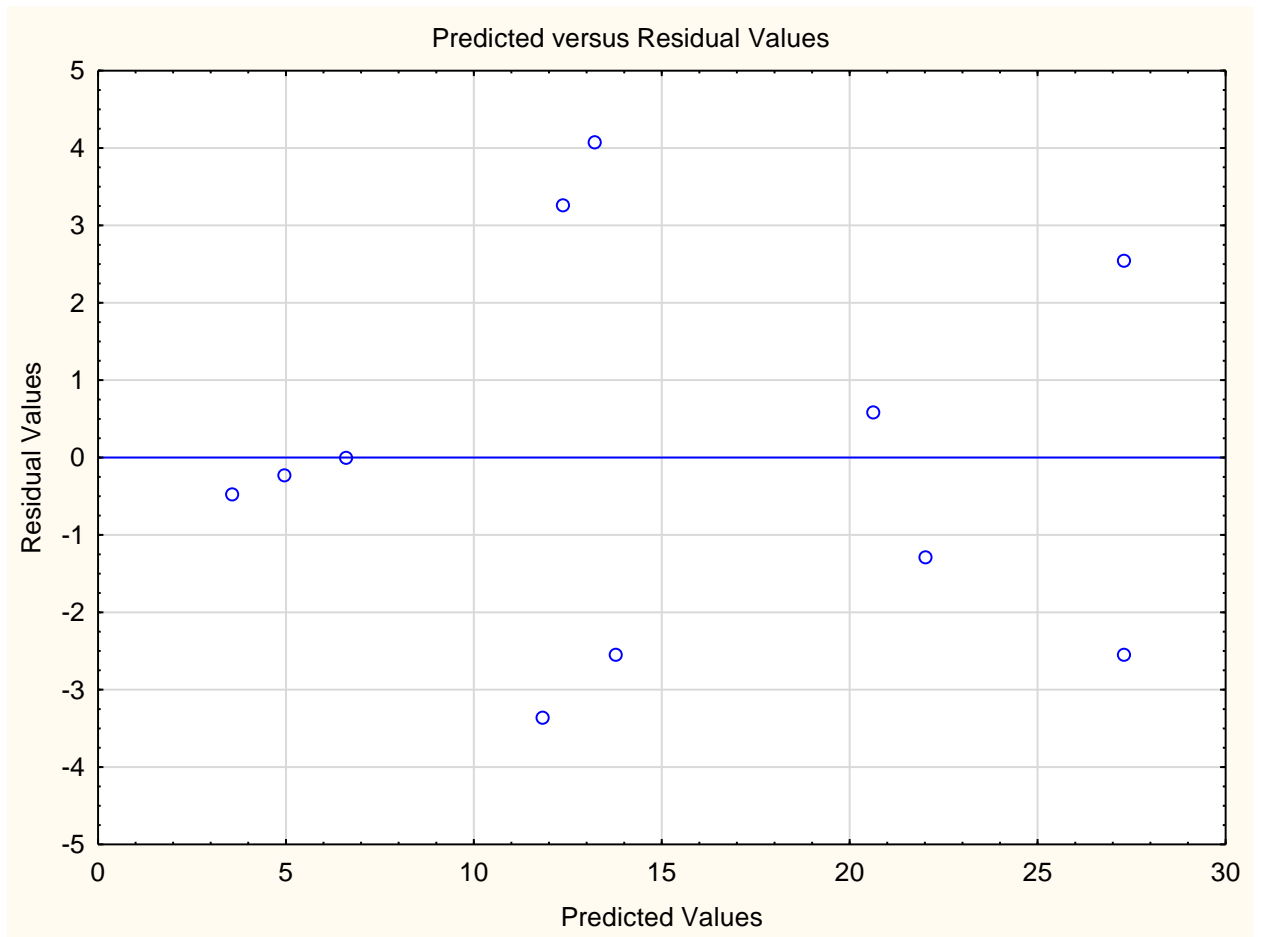


Figure 2. Residual values vs Predicted values obtained with the nonlinear model. The horizontal behavior of blue line suggests an adequate data variation with respect to a central point.

Appendix 6.

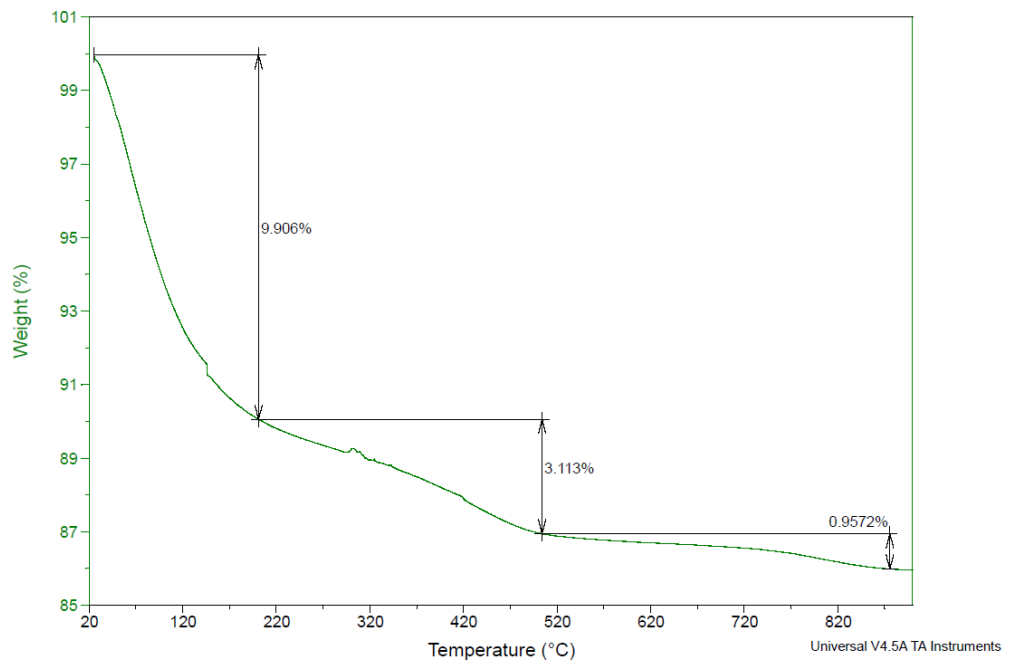


Figure A. Thermogravimetric decomposition Analysis of NH<sub>4</sub>-Mordenite.

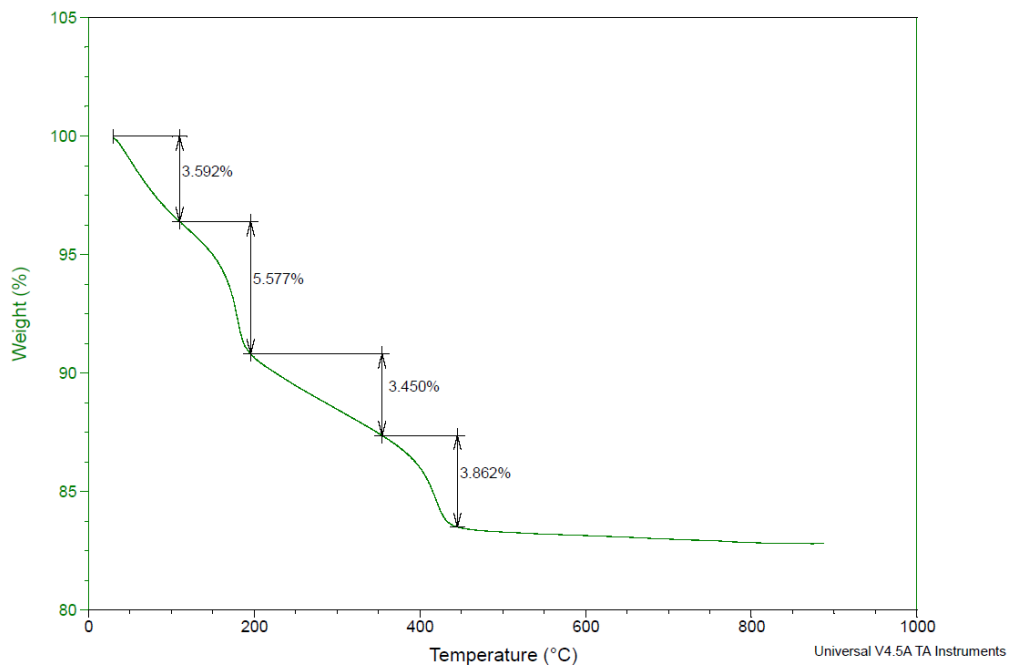


Figure B. Thermogravimetric Decomposition Analysis of CuMor 3%.

## Appendix 7.

### Kubelka-Munk Function.

We employed Diffuse Reflectance Spectra and the data was treated with the Kubelka-Munk (K-M) Function.

$$\frac{k}{S} = \frac{(1 - R_{\infty})^2}{2R_{\infty}} = F(R_{\infty})$$

Where:

K= K-M absorption coefficient.

S= K-M scattering coefficient.

$R_{\infty} = R_{\text{sample}}/R_{\text{standard}}$

The transformation of the diffuse reflectance spectrum to its equivalent in absorbance units is achieved by assuming that the dispersion coefficient S is constant at any wavelength.

## Appendix 8.

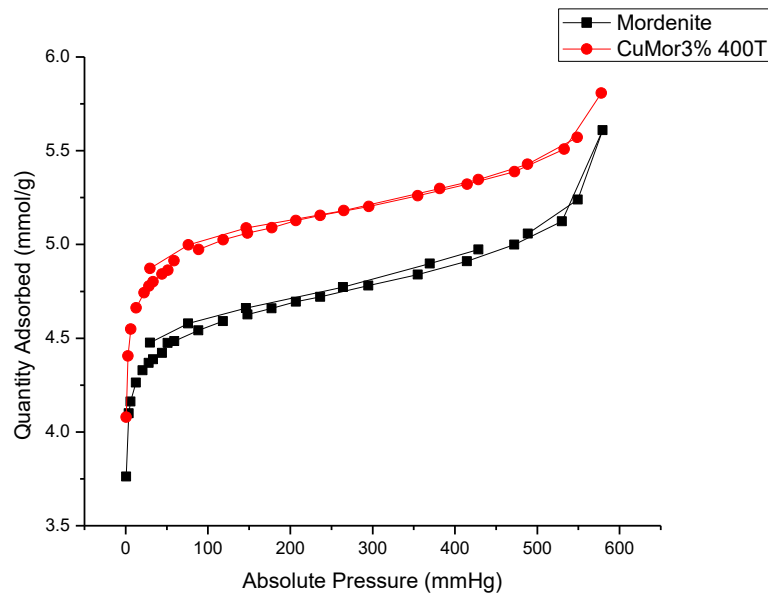


Figure A.8.1. Adsorption Isotherms with Hysteresis of NH<sub>4</sub>.Mordenite and CuMorO<sub>3</sub>% 400T at 74 K.

## Appendix 9.

In order to obtain the methanol yields, it is necessary to find the quantity of methane available to react in 250mg material (through ideal gas equation) for established variables according to each experiment, obtaining the results shown in column *μmol methane (250 mg)*. To calculate the amounts of methanol we employed de GC-MS results (see 3.4.1 table). In order to calculate the methanol yield, we used the corrected t-plot method<sup>88</sup>.

Experimental samples	μmol methane (250 mg)	methanol obtained (μmol/gr)	μmole methanol (250 mg)	μmol methanol (250 mg) Vol Correc total μpore	Methanol Yield (%)
1%300P2	0.939424454	4.732	1.183	1.252565938	94.4
1%300P10	4.697121316	11.215	2.80375	6.262828422	44.8
1%500P2	1.616386978	10.74313169	2.685782923	2.7868741	96.4
1%500P10	8.081933252	20.732	5.183	13.93436768	37.2
5%300P2	0.830273054	3.098	0.7745	1.186104363	65.3
5%300P10	4.15136443	15.636	3.909	5.930520614	65.9
5%500P2	1.717373008	8.46	2.115	3.122496378	67.7
5%500P10	8.5868633	21.206	5.3015	15.61247873	34.0
3%400P6	5.664895622	29.84	7.46	10.29981022	72.4
3%400P6	5.664895622	24.745	6.18625	10.29981022	60.1
1%500P6	4.849160115	6.59	1.6475	8.360620887	19.7